Evaluating the phase diagram at finite isospin and baryon chemical potentials in the Nambu–Jona-Lasinio model

Cheng-fu Mu (穆成富),[1] Lian-yi He (何联毅),[2] and Yu-xin Liu (刘玉鑫)[1,3,*]

[1]*Department of Physics and State Key Laboratory of Nuclear Physics and Technology, Peking University, Beijing 100871, China*
[2]*Frankfurt Institute for Advanced Studies and Institute for Theoretical Physics, J.W. Goethe University, 60438 Frankfurt am Main, Germany*
[3]*Center of Theoretical Nuclear Physics, National Laboratory of Heavy Ion Accelerator, Lanzhou 730000, China*

(Received 20 June 2010; published 10 September 2010)

We study the phase diagram of two-flavor dense QCD at finite isospin and baryon chemical potentials in the framework of the Nambu–Jona-Lasinio model. We focus on the case with arbitrary isospin chemical potential μ_I and small baryon chemical potential $\mu_B \leq \mu_B^\chi$ where μ_B^χ is the critical chemical potential for the first-order chiral phase transition to happen at $\mu_I = 0$. The $\mu_I - \mu_B$ phase diagram shows a rich phase structure since the system undergoes a crossover from a Bose-Einstein condensate of charged pions to a BCS superfluid with condensed quark-antiquark Cooper pairs when μ_I increases at $\mu_B = 0$, and a nonzero baryon chemical potential serves as a mismatch between the pairing species. We observe a gapless pion condensation phase near the quadruple point $(\mu_I, \mu_B) = (m_\pi, M_N - 1.5m_\pi)$ where m_π, M_N are the vacuum masses of pions and nucleons, respectively. The first-order chiral phase transition becomes a smooth crossover when $\mu_I > 0.82m_\pi$. At very large isospin chemical potential, $\mu_I > 6.36m_\pi$, an inhomogeneous Larkin-Ovchinnikov-Fulde-Ferrell superfluid phase, appears in a window of μ_B, which should in principle exist for arbitrary large μ_I. Between the gapless and the Larkin-Ovchinnikov-Fulde-Ferrell phases, the pion superfluid phase and the normal quark matter phase are connected by a first-order phase transition. In the normal phase above the superfluid domain, we find that charged pions are still bound states even though μ_I becomes very large, which is quite different from that at finite temperature. Our phase diagram is in good agreement with that found in imbalanced cold atom systems.

DOI: 10.1103/PhysRevD.82.056006 PACS numbers: 11.30.Qc, 12.39.−x, 21.65.Qr

I. INTRODUCTION

Quantum chromodynamics (QCD) at finite density possesses a richer phase structure than we expected since color superconducting phases can appear at large baryon density due to the attractive color force between quarks [1,2]. However, the lattice simulation of QCD so far can not be successfully carried out at large baryon chemical potential and low temperature due to the sign problem [3], i.e., the fermion determinant is not positive definite in the presence of a nonzero baryon chemical potential μ_B. On the other hand, QCD itself has other conserved charges, such as isospin in the two-flavor case. QCD at finite isospin density, which cannot be realized in a realistic world due to the electromagnetic and weak interactions, serves as an ideal case for lattice study of QCD at finite density [4,5]. Lattice simulation at finite isospin chemical potential μ_I confirms that the system undergoes a second-order phase transition to a pion superfluid phase at a critical isospin chemical potential $\mu_I^c \simeq m_\pi$ where m_π is the pion mass in vacuum [5], which is consistent with the calculations in effective models [6,7]. Isospin matter and pion superfluid have also been studied using holographic QCD models [8]. It is believed that the isospin matter will undergo a smooth crossover from a Bose-Einstein condensate of tightly bound pions to a BCS superfluid with condensed quark-antiquark Cooper pairs [4,9–11]. This crossover is shown to take place at $\mu_I \simeq (2M_N m_\pi^{2/3})^{1/3} \simeq 1.67m_\pi$ [9,10] in the framework of the Nambu–Jona-Lasinio (NJL) model [12] with quarks as elementary blocks. In condensed matter physics, such a phenomenon was discussed many years ago [13] and has been realized in laboratory with cold fermionic atoms via the technology of Fechbach resonance [14]. Possible BEC-BCS crossover and the associated pseudogap phenomenon in the phase diagram of quark matter have been investigated in recent years [15,16].

In addition to the idealized case where fermions form coherent pairs and condense on a uniform Fermi surface, the effect of Zeeman energy splitting H between spin-up and -down electrons on BCS superconductivity was known many years ago [17]. At a critical Zeeman field or the so-called Chandrasekhar-Clogston (CC) limit $H_c = 0.707\Delta_0$ where Δ_0 is the zero temperature gap, a first-order phase transition from the gapped BCS state to the normal state occurs. Further theoretical studies showed that the inhomogeneous Larkin-Ovchinnikov-Fulde-Ferrell (LOFF) state [18,19] may survive in a narrow window between H_c and $H_{LOFF} = 0.754\Delta_0$. However, since the thermodynamic critical field is much smaller than the CC limit due to the strong orbit effect [17], it is hard to observe the CC limit and the LOFF state in ordinary superconductors.

*yxliu@pku.edu.cn

In the scenario of color superconductivity in dense quark matter, the presence of large strange quark mass or isospin chemical potential (equal to the electron chemical potential) due to β-equilibrium naturally serves as a mismatch between the pairing quark species and there is no complex orbit effect since the mismatch is between different quark flavors [20]. The effect of mismatched Fermi surfaces on the ground state of dense quark matter has been investigated in many works [20–22]. However, most of them focus on the weak coupling case. In the scenario of pion superfluidity at finite isospin density, the baryon chemical potential plays naturally the role of mismatch [4,9,23]. The phase structure in the $\mu_I - \mu_B$ plane can be very rich since the system undergoes a BEC-BCS crossover when the isospin chemical potential increases.

The effect of Zeeman splitting or population imbalance on the BEC-BCS crossover has been widely investigated in the cold atom scenario in recent years [24–29]. Theoretical works predict a uniform gapless superfluid phase in the strong coupling (BEC) limit and an inhomogeneous LOFF phase in the weak coupling region [25–28]. However, what occurs in the crossover region is not quite clear. So far the observation of phase separation in cold atom experiments [24] supports the fact that the superfluid phase undergoes a first-order phase transition into the normal phase around the unitary limit and no exotic pairing states are observed there. There also arises a uniform gapless phase, which is called the Sarma phase [30], in the weak coupling region. However, it was found many years ago that the Sarma state corresponds to the maximum of the grand potential and hence is unstable (Sarma instability) [30]. Such a uniform gapless phase promoted great interest due to the work of interior gap superfluidity [31] or breached pairing superfluidity [32]. However, it is found that the stability of such a phase demands special conditions [32]. The appearance of a uniform gapless phase was also predicted in two-flavor dense quark matter, where the Sarma instability can be removed via the charge neutrality constraint [21]. However, it was soon found that the gapless phase suffers from other types of instability, such as imaginary Meissner mass [22] or negative superfluid density [33]. The lesson is that the constraints like charge neutrality in quark matter and fixing particle numbers in cold atoms cannot essentially stabilize the phase which corresponds to the maximum of the grand potential [32,34]. To find the real ground state, one should first study the grand canonical phase diagram with all possible bulk phases with fixed chemical potentials. The bulk phase is stable only when it is built at the global minimum of the grand potential. However, it is not easy to do this, since we may miss some bulk phases in our ansatz and then the analysis is probably not completed.

To shed light on the complete phase diagram of the quark matter at finite isospin and baryon chemical potentials, we investigate the $\mu_I - \mu_B$ phase diagram in the two-flavor Nambu–Jona-Lasinio model in this paper. The NJL model is a suitable model to study BEC-BCS crossover phenomenon at finite isospin density since pions are treated as composite bound objects in the vacuum [35,36]. In our analysis, we include all known bulk phases: uniform superfluid phase, inhomogeneous LOFF phase and normal phase. We also consider possible chiral phase transition [36,37] and quantum phase transition between superfluid phases with different Fermi surface topology [38]. The phase diagram we obtained is shown in Fig. 1. We find that a gapless pion condensed phase (GPC) appears near the quadruple point $(\mu_I, \mu_B) = (m_\pi, M_N - 1.5m_\pi)$. The gapless phase ceases to exist near the BEC-BCS crossover, namely, it exists only in the BEC region.

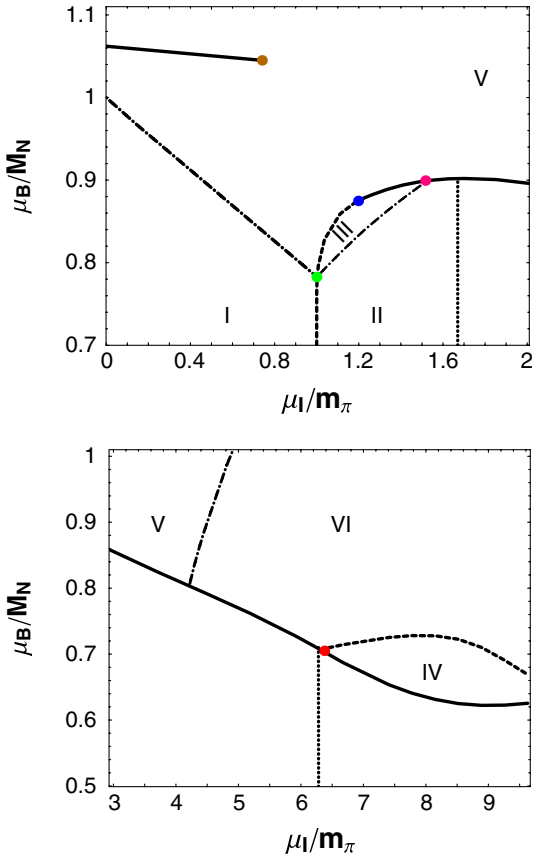

FIG. 1 (color online). Survey of our presently obtained phase diagram of quark matter in terms of the isospin chemical potential (μ_I) and the baryon chemical potential (μ_B) in the two-flavor Nambu–Jona-Lasinio model. The μ_I and μ_B are in unit of pion mass, nucleon mass, respectively. Solid, dashed, and dash-dotted lines stand for first-, second-, and third-order phase transitions, respectively. The Roman numbers denote different phases: I—vacuum, II—pion superfluid, III—gapless pion condensate, IV—LOFF phase, V—normal isospin asymmetric quark matte, and VI—normal quark matter in the presence of a Fermi surface for antiquarks. The dotted lines represent the BEC-BCS crossover. The BEC (BCS) region is located on the left (right) of the dotted line in the upper (lower) panel, respectively. Between the BEC and BCS domains the superfluid matter is in a crossover state.

In particular, the phase diagram near the quadruple point is quite similar to that found in cold fermionic atoms [26]. At very large isospin chemical potential, $\mu_I > 6.36 m_\pi$, an inhomogeneous LOFF superfluid phase appears in a window of μ_B, which should in principle exist for arbitrary large μ_I. Between the gapless and LOFF phases, the pion superfluid phase and the normal quark matter phase are connected by a simple first-order phase transition. We also observe that the first-order chiral phase transition turns out to be a smooth crossover when $\mu_I > 0.82 m_\pi$.

The paper is organized as follows. In Sec. II, we review the formalism of pion condensation in the NJL model at finite isospin chemical potential μ_I and baryon chemical potential μ_B, and explain the BEC-BCS crossover phenomenon when μ_I increases. In Sec. III, we investigate the phase diagram near the critical isospin chemical potential $\mu_I = m_\pi$ and discuss the possible quantum phase transition and chiral phase transition. In Sec. IV, we evaluate the inhomogeneous LOFF phase at large μ_I. In Sec. V, we discuss the properties of charged pion modes in the normal quark matter phase. Finally, in Sec. VI, we give a summary.

II. NJL MODEL AT FINITE ISOSPIN CHEMICAL POTENTIAL μ_I: FROM PION TO QUARK–ANTIQUARK CONDENSATES

We first review in this section the Nambu–Jona-Lasinio (NJL) model description of QCD at finite isospin density [7]. The Lagrangian density of the two-flavor NJL model is defined as

$$\mathcal{L}_{\rm NJL} = \bar\psi(i\gamma^\mu\partial_\mu - m_0)\psi + G[(\bar\psi\psi)^2 + (\bar\psi i\gamma_5\boldsymbol{\tau}\psi)^2]. \tag{1}$$

Here the current quark mass m_0, the coupling constant G and a momentum cutoff Λ are model parameters determined by QCD vacuum phenomenology. The scalar and pseudoscalar interactions in the bracket correspond to σ-meson and pion excitations. For vanishing current quark mass m_0, the NJL Lagrangian possesses the same global symmetry $U_B(1) \otimes SU_L(2) \otimes SU_R(2)$ as the QCD Lagrangian, corresponding to baryon number symmetry, isospin symmetry and chiral symmetry, respectively. In the physics vacuum, the symmetry $SU_L(2) \otimes SU_R(2)$ is spontaneously broken down to $SU_{L+R}(2)$ by a nonzero chiral condensate $\langle\bar\psi\psi\rangle \neq 0$, associated with three massless pions as the Goldstone bosons. In the presence of a small nonzero current quark mass, the pions become pseudo-Goldstone bosons with a mass much smaller than other hadrons.

To calculate the effective action at finite chemical potential and finite temperature, we start with the partition function defined as

$$Z_{\rm NJL}(T, V, \mu_I, \mu_B) = \int [d\bar\psi][d\psi] \times \exp\Big[\int_0^\beta d\tau \int d^3\mathbf{r}(\mathcal{L}_{\rm NJL} + \bar\psi\,\hat\mu\,\gamma_0\psi)\Big], \tag{2}$$

where $\hat\mu = {\rm diag}(\mu_u, \mu_d)$ is the chemical potential matrix and the chemical potentials for u- and d-quarks are defined as

$$\mu_u = \frac{\mu_B}{N_c} + \frac{\mu_I}{2}, \qquad \mu_d = \frac{\mu_B}{N_c} - \frac{\mu_I}{2}, \tag{3}$$

with $N_c = 3$, the number of color. Here μ_I, μ_B is the isospin chemical potential, the baryon chemical potential introduced corresponding to the conserved isospin charge $I_3 = \int d^3\mathbf{r}\,\bar\psi\gamma_0\tau_3\psi/2$, and the baryon number $B = \int d^3\mathbf{r}\,\bar\psi\gamma_0\psi/N_c$, respectively. For the case at small enough baryon chemical potential, $\mu_B < \mu_B^\chi$, where μ_B^χ is the critical baryon chemical potential for the first-order chiral phase transition to take place at $\mu_I = 0$, we do not consider the possibility of a diquark condensate. The effective action for a four-fermion interaction theory can be derived using a modern functional integral method. Introducing the auxiliary meson fields $\sigma(\tau, \mathbf{r})$ and $\boldsymbol{\pi}(\tau, \mathbf{r})$, which satisfy the equations of motion $\sigma = -2G\bar\psi\psi$, $\boldsymbol{\pi} = -2G\bar\psi i\gamma_5\boldsymbol{\tau}\psi$, respectively, we obtain from the Stratonovich-Hubbard transformation

$$\begin{aligned} Z_{\rm NJL}(T, V, \mu_I, \mu_B) &= \int [d\bar\psi][d\psi][d\sigma][d\boldsymbol{\pi}] \exp\Big\{\int_0^\beta d\tau \int d^3\mathbf{r}\,\mathcal{L}_{\rm eff}[\bar\psi, \psi, \sigma, \boldsymbol{\pi}]\Big\}, \\ \mathcal{L}_{\rm eff}[\bar\psi, \psi, \sigma, \boldsymbol{\pi}] &= \bar\psi\,\mathcal{K}[\sigma, \boldsymbol{\pi}]\psi - \frac{\sigma^2 + \boldsymbol{\pi}2}{4G}, \\ \mathcal{K}[\sigma, \boldsymbol{\pi}] &= i\gamma^\mu\partial_\mu - m_0 + \frac{\mu_I}{2}\gamma_0\tau_3 + \frac{\mu_B}{N_c}\gamma_0 - (\sigma + i\gamma_5\boldsymbol{\tau}\cdot\boldsymbol{\pi}). \end{aligned} \tag{4}$$

Integrating out the quark degree of freedom, we obtain the effective action including only bosonic degrees of freedom as

$$Z_{\rm NJL}(T, V, \mu_I, \mu_B) = \int [d\sigma][d\boldsymbol{\pi}] e^{-\mathcal{S}_{\rm eff}[\sigma, \boldsymbol{\pi}]}, \tag{5}$$

with

$$\mathcal{S}_{\rm eff}[\sigma, \boldsymbol{\pi}] = \int_0^\beta d\tau \int d^3\mathbf{r}\frac{\sigma^2 + \boldsymbol{\pi}2}{4G} - {\rm Tr}\ln\mathcal{K}[\sigma, \boldsymbol{\pi}]. \tag{6}$$

To make the physical picture more clear, we define the charged pion fields $\pi_\pm(\tau, \mathbf{r}) = (\pi_1 \pm i\pi_2)/\sqrt{2}$, or the

auxiliary pairing fields $\Phi(\tau, \mathbf{r})$ and $\Phi^*(\tau, \mathbf{r})$, as those in BCS theory,

$$\begin{aligned}\Phi(\tau, \mathbf{r}) &= \sqrt{2}\pi_+(\tau, \mathbf{r}) = -4G\bar{u}i\gamma_5 d,\\ \Phi^*(\tau, \mathbf{r}) &= \sqrt{2}\pi_-(\tau, \mathbf{r}) = -4G\bar{d}i\gamma_5 u.\end{aligned} \tag{7}$$

Then the two-flavor forms a Nambu-Gorkov space like in the relativistic BCS theory [2]. In this space, the fermion matrix $\mathcal{K}$ can be expressed in a BCS form

$$\mathcal{K} = \begin{pmatrix} i\gamma^\mu\partial_\mu - m_0 + \left(\frac{\mu_B}{N_c} + \frac{\mu_I}{2}\right)\gamma_0 - \sigma - i\gamma_5\pi_0 & -i\gamma_5\Phi \\ -i\gamma_5\Phi^* & i\gamma^\mu\partial_\mu - m_0 + \left(\frac{\mu_B}{N_c} - \frac{\mu_I}{2}\right)\gamma_0 - \sigma + i\gamma_5\pi_0 \end{pmatrix}. \tag{8}$$

The effective action cannot be evaluated exactly in the 3 + 1 dimension. In this paper we adopt the $1/N_c$ expansion. First we consider the zeroth order of the effective action, where the auxiliary meson fields are replaced by their expectation values, which are determined by the saddle point conditions,

$$\frac{\delta\mathcal{S}_{\text{eff}}[\sigma, \boldsymbol{\pi}]}{\delta\sigma} = 0, \qquad \frac{\delta\mathcal{S}_{\text{eff}}[\sigma, \boldsymbol{\pi}]}{\delta\boldsymbol{\pi}} = 0. \tag{9}$$

In the vacuum, the ansatz for the expectation values of the composite meson field $\bar{\psi}\psi$ and $\bar{\psi}i\gamma_5\boldsymbol{\tau}\psi$ are taken to be $\langle\bar{\psi}\psi\rangle \neq 0$ and $\langle\bar{\psi}i\gamma_5\boldsymbol{\tau}\psi\rangle = 0$, which means the spontaneous breaking of the chiral symmetry when $m_0 = 0$. However, in presence of a nonzero isospin chemical potential μ_I, the original symmetry group $\mathrm{SU_L}(2) \otimes \mathrm{SU_R}(2)$ at $m_0 = 0$ explicitly breaks down to a subgroup $\mathrm{U_L}(1) \otimes \mathrm{U_R}(1) \simeq \mathrm{U_I}(1) \otimes \mathrm{U_{IA}}(1)$, with the generator being the third component of the isospin charge $\mathbf{I}_3$ and the corresponding field transformation being $\psi \rightarrow e^{-i\alpha\tau_3/2}\psi$ and $\psi \rightarrow e^{-i\gamma_5\alpha'\tau_3/2}\psi$. Thus at sufficiently large μ_I, we should consider the possibility $\langle\bar{\psi}i\gamma_5\tau_3\psi\rangle = 0$ and $\langle\bar{u}i\gamma_5 d\rangle \neq 0$, which further breaks the $\mathrm{U_I}(1)$ symmetry and corresponds to a Bose condensate of charged pions at low density. Thus we take the following Ansätze for the field expectation values:

$$\begin{aligned}\langle\bar{\psi}\psi\rangle &= \langle\bar{u}u\rangle + \langle\bar{d}d\rangle \neq 0,\\ \langle\bar{u}i\gamma_5 d\rangle &= \langle\bar{d}i\gamma_5 u\rangle^* \neq 0.\end{aligned} \tag{10}$$

Equivalently, we write

$$\upsilon = \langle\sigma\rangle = -2G\langle\bar{\psi}\psi\rangle, \tag{11}$$

and

$$\begin{aligned}\langle\Phi\rangle &= -4G\langle\bar{u}i\gamma_5 d\rangle = \Delta e^{i\theta},\\ \langle\Phi^*\rangle &= -4G\langle\bar{d}i\gamma_5 u\rangle = \Delta e^{-i\theta}.\end{aligned} \tag{12}$$

Here the phase angle θ of the condensate corresponds to the direction of spontaneous breaking of $\mathrm{U_I}(1)$ symmetry. For a homogeneous ground state, we can consider $\theta = 0$ without loss of generality, which is equivalent to the gauge

$$\langle\bar{\psi}i\gamma_5\tau_1\psi\rangle = -\frac{\Delta}{2G}, \qquad \langle\bar{\psi}i\gamma_5\tau_2\psi\rangle = 0. \tag{13}$$

Once the expectation values υ and Δ are determined by the stationary conditions, one can evaluate the effective action around the mean field to higher order, corresponding to mesonic fluctuations. In this paper, we focus on the phase structure at zero temperature and the effect of mesonic fluctuations will not be taken into account. At finite temperature, the effect of mesonic fluctuations may be significant.

Let us at first discuss the $\mu_B = 0$ case. At zero temperature, the zeroth order effective action $\mathcal{S}^{(0)}_{\text{eff}}$ or the mean field thermodynamic potential $\Omega = \mathcal{S}^{(0)}_{\text{eff}}/\beta V$ ($V \rightarrow \infty$ is the volume of the system) can be evaluated as

$$\begin{aligned}\Omega(M, \Delta) = &\frac{(M - m_0)^2 + \Delta^2}{4G} - 2N_c\int^\Lambda \frac{d^3\mathbf{k}}{(2\pi)^3}\\ &\times\left[\sqrt{\left(E_{\mathbf{k}} - \frac{\mu_I}{2}\right)^2 + \Delta^2} + \sqrt{\left(E_{\mathbf{k}} + \frac{\mu_I}{2}\right)^2 + \Delta^2}\right],\end{aligned} \tag{14}$$

where $E_{\mathbf{k}} = \sqrt{\mathbf{k}^2 + M^2}$ with the dynamical quark mass $M = m_0 + \upsilon$. Here we employ a three-momentum cutoff Λ to regularize the integral. In the numerical calculations, we take $m_0 = 5$ MeV, $G = 4.93$ GeV^{-2} and $\Lambda = 653$ MeV, which fit the pion mass $m_\pi = 134$ MeV, pion decay constant $f_\pi = 93$ MeV, and the chiral condensate $\langle\bar{u}u\rangle = (-250\ \text{MeV})^3$ in the vacuum [35]. In this case, we have a constituent quark mass $M^* = 313$ MeV $= M_N/3$ in the vacuum.

The ground state at finite μ_I is determined by minimizing the effective potential (in Eq. (14)) with respect to M and Δ, or solving the equations of the saddle point conditions (in Eq. (9)). The numerical results are shown in Fig. 2(a). Independent of the model parameter set, there exists a second-order phase transition from the vacuum to a pion superfluid phase with $\Delta \neq 0$ at a critical isospin chemical potential exactly equal to the vacuum pion mass m_π, and the chiral quark condensate as well as the dynamical quark mass decrease gradually with the increase of μ_I, which in our numerical results is in good agreement

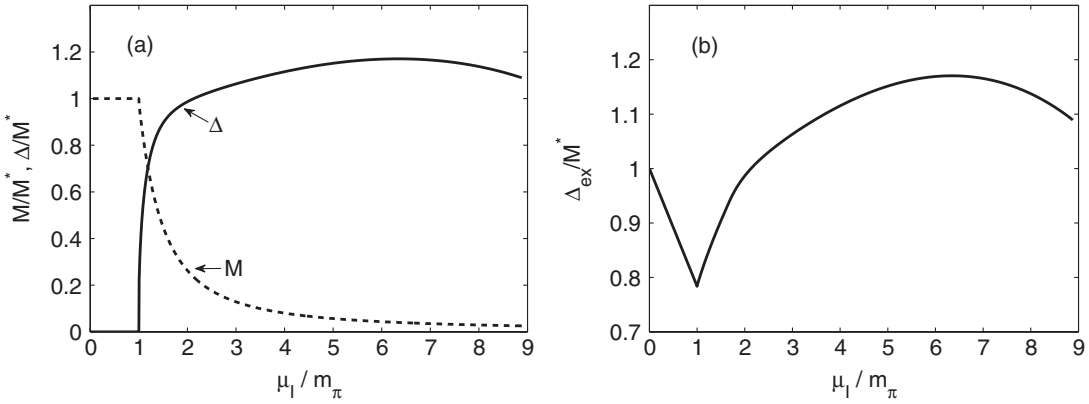

FIG. 2. (a) The isospin chemical potential μ_I dependence of the dynamical quark mass M and the superfluid order parameter Δ (the M and Δ are in unit of the dynamical quark mass M^* in vacuum, the μ_I is in unit m_π). (b) The isospin chemical potential μ_I dependence of the single-particle excitation gap Δ_{ex} (in unit M^*).

with the chiral rotation behavior $\langle\bar{\psi}\psi\rangle_{\mu_I}/\langle\bar{\psi}\psi\rangle_0 = m_\pi^2/\mu_I^2$ [4].

To investigate the single-particle (quark) excitation spectrum, one has to know the quark propagator. The quark propagator $\mathcal{G}(i\omega_n, \mathbf{k})$ in momentum space can be evaluated as

$$\begin{aligned}\mathcal{G}(i\omega_n, \mathbf{k}) = &\frac{1}{(i\omega_n)^2 - (E_{\mathbf{k}}^-)^2} \\ &\times \begin{pmatrix} (i\omega_n + \xi_{\mathbf{k}}^-)\Lambda_{\mathbf{k}}^+\gamma_0 & -i\Delta\Lambda_{\mathbf{k}}^+\gamma_5 \\ -i\Delta\Lambda_{\mathbf{k}}^-\gamma_5 & (i\omega_n - \xi_{\mathbf{k}}^-)\Lambda_{\mathbf{k}}^-\gamma_0 \end{pmatrix} \\ &+ \frac{1}{(i\omega_n)^2 - (E_{\mathbf{k}}^+)^2} \\ &\times \begin{pmatrix} (i\omega_n - \xi_{\mathbf{k}}^+)\Lambda_{\mathbf{k}}^-\gamma_0 & -i\Delta\Lambda_{\mathbf{k}}^-\gamma_5 \\ -i\Delta\Lambda_{\mathbf{k}}^+\gamma_5 & (i\omega_n + \xi_{\mathbf{k}}^+)\Lambda_{\mathbf{k}}^+\gamma_0 \end{pmatrix},\end{aligned} \tag{15}$$

with the notations $E_{\mathbf{k}}^\pm = [(\xi_{\mathbf{k}}^\pm)^2 + \Delta^2]^{1/2}$, $\xi_{\mathbf{k}}^\pm = E_{\mathbf{k}} \pm \mu_I/2$, and the massive energy projector $\Lambda_{\mathbf{k}}^\pm = \frac{1}{2} \times (1 \pm \frac{\gamma_0(\boldsymbol{\gamma}\cdot\mathbf{k}+M)}{E_{\mathbf{k}}})$. The quasiparticle excitation spectrum is given by the poles of the propagator,

$$\begin{aligned}\omega_{1,2}(\mathbf{k}) &= \pm\sqrt{\left(E_{\mathbf{k}} - \frac{\mu_I}{2}\right)^2 + \Delta^2}, \\ \omega_{3,4}(\mathbf{k}) &= \pm\sqrt{\left(E_{\mathbf{k}} + \frac{\mu_I}{2}\right)^2 + \Delta^2}.\end{aligned} \tag{16}$$

The single-particle excitation gap Δ_{ex} is defined by the minimum of the above dispersions, $\Delta_{ex} = \min_{\mathbf{k}}\{|\omega_{1,2,3,4}|\}$, and can be written in a compact form

$$\Delta_{ex}(\mu_I) = \sqrt{\left(M_0 - \frac{\mu_I}{2}\right)^2\Theta\left(M_0 - \frac{\mu_I}{2}\right) + \Delta_0^2}, \tag{17}$$

where M_0 and Δ_0 stand for the real minimum of the grand potential at $\mu_B = 0$. It is indeed the excitation gap of the branch $\omega_{1,2}$. The numerical results of its isospin chemical potential dependence are shown in Fig. 2(b). It is apparent that there is a characteristic change of the excitation spectrum at another critical isospin chemical potential μ_I^0 defined by the relation $M(\mu_I) = \mu_I/2$. Using the chiral rotation behavior of $M(\mu_I)$, one finds $\mu_I^0 = (2M^* m_\pi^2)^{1/3}$. For our model parameter set we obtain $\mu_I^0 = 1.67 m_\pi$, which is in good agreement with the numerical results.

In the case $m_\pi < \mu_I < \mu_I^0$, the minimum of the dispersions $|\omega_{1,2}|$ is still located at $|\mathbf{k}| = 0$, and the excitation gap is not equal to the superfluid order parameter, $\Delta_{ex} = [(M_0 - \mu_I/2)^2 + \Delta_0^2]^{1/2}$. While for $\mu_I > \mu_I^0$, the minimum is shifted to a nonzero momentum $|\mathbf{k}| = (\mu_I^2/4 - M_0^2)^{1/2}$ which leads to a BCS-like behavior, and the excitation gap becomes equal to the superfluid order parameter Δ_0. Such a behavior, in the condensed matter physics point of view [13,25], indicates that the system undergoes a BCS-BEC crossover at approximately $\mu_I = \mu_I^0$. Approaching the BEC limit $\mu_I \to m_\pi$, the ground state is indeed a Bose condensate of weakly repulsive pions of which the equation of state is shown to be consistent with the Lee-Huang-Yang theory with a repulsive scattering length $a = m_\pi/(16\pi f_\pi^2)$ even within the NJL mean field [39]. In the opposite limit $\mu_I \gg m_\pi$, the ground state should be a BCS superfluid with condensed quark-antiquark Cooper pairs [4]. In our NJL approach, the real BCS limit cannot be reached, and in a wide region of μ_I, the system should be in a strongly coupled BCS state.

III. PHASE STRUCTURE NEAR $\mu_I = m_\pi$: GAPLESS PION CONDENSATE

We now turn on a nonzero baryon chemical potential μ_B. In this case, the quark propagator $\mathcal{G}(i\omega_n, \mathbf{k})$ in momentum space takes the same form as Eq. (15) but with the replacement $i\omega_n \to i\omega_n + H$ where we have defined $H \equiv \mu_B/N_c$. Then the quasiparticle excitation spectra read

$$\begin{aligned}
\omega_1(\mathbf{k}) &= \sqrt{\left(E_{\mathbf{k}} - \frac{\mu_I}{2}\right)^2 + \Delta^2} - H, \\
\omega_2(\mathbf{k}) &= -\sqrt{\left(E_{\mathbf{k}} - \frac{\mu_I}{2}\right)^2 + \Delta^2} - H, \\
\omega_3(\mathbf{k}) &= \sqrt{\left(E_{\mathbf{k}} + \frac{\mu_I}{2}\right)^2 + \Delta^2} - H, \\
\omega_4(\mathbf{k}) &= -\sqrt{\left(E_{\mathbf{k}} + \frac{\mu_I}{2}\right)^2 + \Delta^2} - H.
\end{aligned} \tag{18}$$

Unlike the case of $\mu_B = 0$ where all quasiparticles are gapped, it is now possible to find gapless quasiparticles with nonvanishing superfluid order parameter Δ. The gapless quasiparticles appear when the mismatch H satisfies the relation

$$H > \sqrt{\left(M - \frac{\mu_I}{2}\right)^2 \Theta\left(M - \frac{\mu_I}{2}\right) + \Delta^2}, \tag{19}$$

where M and Δ are the solutions which minimize the grand potential at given H. Since we consider $\mu_B > 0$ without loss of generality, only branches ω_1 and ω_3 are possible candidates for the gapless quasiparticles. All possible gapless phases can be sorted via defining the following possible gapless surfaces in momentum space:

$$k_1 = M\sqrt{\lambda_1^2 - 1}, \qquad k_2 = M\sqrt{\lambda_2^2 - 1}, \tag{20}$$

with

$$\lambda_1 = \frac{\mu_I/2 - \sqrt{H^2 - \Delta^2}}{M}, \qquad \lambda_2 = \frac{\mu_I/2 + \sqrt{H^2 - \Delta^2}}{M}. \tag{21}$$

Then we have the following three possible types of gapless phases. *Type 1*: $|\lambda_1| < 1$ and $|\lambda_2| > 1$. In this case, only the branch ω_1 has one gapless node k_2; the other branches are all gapped.

Type 2: $\lambda_1 > 0$ and $|\lambda_{1,2}| > 1$. In this case, only the branch ω_1 has two gapless nodes k_1 and k_2; the other branches are all gapped.

Type 3: $\lambda_1 < 0$ and $|\lambda_{1,2}| > 1$. In this case, the branch ω_1 has a gapless node k_2, and the branch ω_3 has a gapless node k_1; the other branches are all gapped.

In this section, we focus on the BEC region where $\mu_I \gtrsim m_\pi$. Since $M > \mu_I/2$, we have $|\lambda_1| < 1$ and hence the possible gapless phase should be of Type 1. This can be understood by the BEC nature of the quasiparticles. At $H = 0$, the minimum of the dispersion $|\omega_2|$ is located at $k = 0$, then a nonzero H will shift the dispersion to cross the $\omega = 0$ axis. We call this phase the gapless pion condensate (GPC).

A. Phase diagram: Numerical results

To identify the appearance of the GPC phase in the $\mu_I - \mu_B$ phase diagram, we analyze the behavior of the effective potential $\Omega(M, \Delta)$ with increasing H. At finite baryon chemical potential μ_B, the effective action can be written as

$$\begin{aligned}
\Omega(M,\Delta) = {} & \frac{(M - m_0)^2 + \Delta^2}{4G} - 2N_c \int^\Lambda \frac{d^3\mathbf{k}}{(2\pi)^3} \times \left[\sqrt{\left(E_{\mathbf{k}} - \frac{\mu_I}{2}\right)^2 + \Delta^2} + \sqrt{\left(E_{\mathbf{k}} + \frac{\mu_I}{2}\right)^2 + \Delta^2}\right] \\
& + 2N_c \int^\Lambda \frac{d^3\mathbf{k}}{(2\pi)^3} \left(\sqrt{\left(E_{\mathbf{k}} - \frac{\mu_I}{2}\right)^2 + \Delta^2} - H\right) \Theta\left(H - \sqrt{\left(E_{\mathbf{k}} - \frac{\mu_I}{2}\right)^2 + \Delta^2}\right) \\
& + 2N_c \int^\Lambda \frac{d^3\mathbf{k}}{(2\pi)^3} \left(\sqrt{\left(E_{\mathbf{k}} - \frac{\mu_I}{2}\right)^2 + \Delta^2} + H\right) \Theta\left(-H - \sqrt{\left(E_{\mathbf{k}} - \frac{\mu_I}{2}\right)^2 + \Delta^2}\right) \\
& + 2N_c \int^\Lambda \frac{d^3\mathbf{k}}{(2\pi)^3} \left(\sqrt{\left(E_{\mathbf{k}} + \frac{\mu_I}{2}\right)^2 + \Delta^2} - H\right) \Theta\left(H - \sqrt{\left(E_{\mathbf{k}} + \frac{\mu_I}{2}\right)^2 + \Delta^2}\right) \\
& + 2N_c \int^\Lambda \frac{d^3\mathbf{k}}{(2\pi)^3} \left(\sqrt{\left(E_{\mathbf{k}} + \frac{\mu_I}{2}\right)^2 + \Delta^2} + H\right) \Theta\left(-H - \sqrt{\left(E_{\mathbf{k}} + \frac{\mu_I}{2}\right)^2 + \Delta^2}\right).
\end{aligned} \tag{22}$$

According to our discussion above, the last three terms do not contribute to the GPC and can be safely neglected. Analyzing the variation behavior of the thermodynamic potential $\Omega(M, \Delta)$ with respect to H, we can determine the phase boundary between the superfluid phase (with $\Delta \neq 0$) and the normal phase (with $\Delta = 0$) according the Landau criterion of phase transition.

The numerical result of the phase diagram in terms of μ_I and μ_B in our model parameter set is illustrated in Fig. 3.

It is evident that there exist four phases in the phase diagram: (1) the pion condensed phase with gapped single-particle excitations; (2) the gapless pion condensate with gapless single-particle excitations; (3) the normal phase with nonzero baryon density; and (4) the vacuum with zero baryon density.

The superfluid to normal phase transition is second order when μ_I approaches m_π, but becomes first order when μ_I exceeds a critical value, which means that the point at the

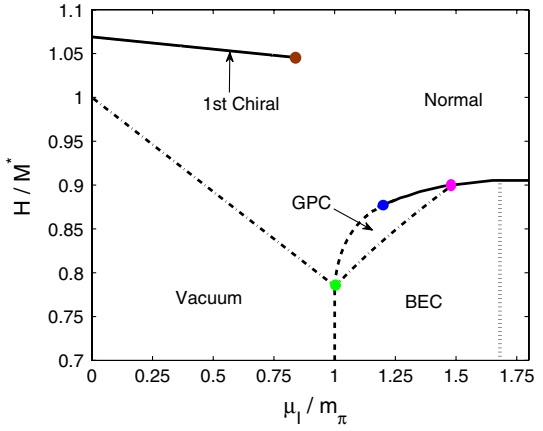

FIG. 3 (color online). Calculated phase diagram in terms of $\mu_{\rm I}$ and $\mu_{\rm B}$ near the critical isospin chemical potential $\mu_{\rm I}^c = m_\pi$.

superfluid-normal phase boundary shown by a blue dot in Fig. 3 is a tricritical point. For several model parameter sets used in literature, we find that the value of $\mu_{\rm I}$ at the tricritical point is less than $\mu_{\rm I}^0$ where BCS-BEC crossover takes place. While the location of the tricritical point is model-parameter dependent, its appearance seems unavoidable, since at small enough H ($H < M^* - m_\pi/2$, see below) the vacuum-superfluid phase transition which takes place at $\mu_{\rm I} = m_\pi$ should be of second order, and at large $\mu_{\rm I}$ the superfluid-normal phase transition is well known of first order.

On the other hand, the superfluid domain can be separated into the BEC phase with gapped single-particle excitations and the GPC phase with gapless single-particle excitations according to the criterion in Eq. (19). The boundary which denotes the gapped-gapless transition is shown in Fig. 3 by a dash-dotted line above the BEC region. According to the Landau criterion, there may not exist a phase transition since the superfluid order parameter does not undergo a characteristic change. However, as we will show below, there does exist a third-order phase transition from the BEC phase to the gapless phase. An interesting phenomenon is that the BEC-GPC phase transition takes place just when the mismatch H becomes equal to the single-particle excitation gap $\Delta_{\rm ex}(\mu_{\rm I})$ at $H = 0$. That is, if we use the dimensionless parameter $\eta = H/\Delta_{\rm ex}(\mu_{\rm I})$ on the vertical axis, as employed in Ref. [25], the BEC-GPC phase transition takes place just at $\eta = 1$. At $\mu_{\rm I} = m_\pi$ we have $\Delta_{\rm ex} = M^* - m_\pi/2$, hence all the four phases (BEC, GPC, normal, and vacuum) meet at a quadruple point $(\mu_{\rm I}, H) = (m_\pi, M^* - m_\pi/2)$ shown by a green dot in Fig. 3. At larger isospin chemical potential, the window of the gapless phase becomes closed, and the gapped-gapless boundary and the first-order phase transition line meet at a triple point shown by a pink dot in Fig. 3.

On the other side $\mu_{\rm I} < m_\pi$, there exists a first-order chiral phase transition line which ends up at a critical endpoint shown by a brown dot in Fig. 3 and a third-order phase transition line which separates the vacuum with zero baryon density and the normal matter phase with nonzero baryon density. The latter transition, which in realistic QCD may be replaced by a first-order phase transition, has the same nature as the BEC-GPC phase transition. The two-flavor color superconducting (2SC) phase can appear above the first-order chiral phase transition line, and disappears when $\mu_{\rm I}$ becomes sufficiently large since $\mu_{\rm I}$ plays the role of Fermi surface mismatch between u and d quarks. For a simple estimation, we adopt the color superconducting gap to be $\Delta_{\rm csc} \sim 100$ MeV at $H \sim$ (300–500) MeV, the 2SC phase thus disappears at $\mu_{\rm I}/2 \simeq 0.707\Delta_{\rm csc} \sim 70$ MeV. Therefore, our phase diagram will not change even though the 2SC phase is taken into account.

B. Superfluid-normal phase transition and tricritical point

To ensure the existence of a tricritical point and give a more precise determination of its location, we implement the Ginzburg-Landau theory. Keep in mind that near the second-order phase transition, the superfluid order parameter Δ approaches zero continuously and the dynamical quark mass M can be treated as a function of Δ^2 through the gap equation $\partial\Omega/\partial M = 0$. Since the grand potential is a function of Δ^2, we can write $\Omega = \Omega(\Delta^2, M(\Delta^2))$ and the chemical potentials $\mu_{\rm I}$ and $\mu_{\rm B}$ can be treated as external parameters.

Expanding the grand potential in terms of Δ^2 up to the order Δ^6, we have

$$\Omega(\Delta^2, M(\Delta^2)) = \Omega(0, M(0)) + \frac{1}{2}\alpha\Delta^2 + \frac{1}{4}\beta\Delta^4 + \frac{1}{6}\gamma\Delta^6. \quad (23)$$

The coefficients α, β and γ can be derived from the derivative expansion method based on the path integral representation in Eq. (5), however, more directly from the grand potential in Eq. (22). Taking the definition of the Taylor expansion and the gap equation $\partial\Omega/\partial M = 0$ into account, we obtain

$$\frac{\alpha}{2} = \frac{d\Omega}{d\Delta^2} = \frac{\partial\Omega}{\partial\Delta^2} + \frac{\partial\Omega}{\partial M}\frac{dM}{d\Delta^2} = \frac{\partial\Omega}{\partial\Delta^2},$$
$$\frac{\beta}{2} = \frac{d^2\Omega}{d(\Delta^2)^2} = \frac{\partial^2\Omega}{\partial(\Delta^2)^2} + \frac{\partial^2\Omega}{\partial\Delta^2\partial M}\frac{dM}{d\Delta^2}. \quad (24)$$

All derivatives should take their values at $\Delta = 0$, but we neglect this notation here and in the following. To evaluate the quantity $dM/d\Delta^2$, we employ the derivative of the gap equation $\partial\Omega/\partial M = 0$ with respect to Δ^2 and find

$$\frac{\partial}{\partial\Delta^2}\frac{\partial\Omega}{\partial M} + \frac{\partial}{\partial M}\left(\frac{\partial\Omega}{\partial M}\right)\frac{dM}{d\Delta^2} = 0. \quad (25)$$

We obtain then

$$\frac{\beta}{2} = \frac{\partial^2\Omega}{\partial(\Delta^2)^2} - \left(\frac{\partial^2\Omega}{\partial\Delta^2\partial M}\right)^2\left(\frac{\partial^2\Omega}{\partial M^2}\right)^{-1}. \quad (26)$$

Thus the coefficients α and β can be calculated with the following results:

$$\begin{aligned}
\frac{\partial\Omega}{\partial\Delta^2} &= \frac{1}{4G} - N_c\sum_{e=\pm}\int^{\Lambda}\frac{d^3\mathbf{k}}{(2\pi)^3}\frac{\Theta(H+\xi^e_{\mathbf{k}})-\Theta(H-\xi^e_{\mathbf{k}})}{\xi^e_{\mathbf{k}}},\\
\frac{\partial^2\Omega}{\partial(\Delta^2)^2} &= \frac{N_c}{2}\sum_{e=\pm}\int^{\Lambda}\frac{d^3\mathbf{k}}{(2\pi)^3}\left[\frac{\Theta(H+\xi^e_{\mathbf{k}})-\Theta(H-\xi^e_{\mathbf{k}})}{(\xi^e_{\mathbf{k}})^3}-\frac{\delta(H-\xi^e_{\mathbf{k}})+\delta(H+\xi^e_{\mathbf{k}})}{(\xi^e_{\mathbf{k}})^2}\right],\\
\frac{\partial^2\Omega}{\partial\Delta^2\partial M} &= N_c\sum_{e=\pm}\int^{\Lambda}\frac{d^3\mathbf{k}}{(2\pi)^3}\frac{M}{E_{\mathbf{k}}}\left[\frac{\Theta(H+\xi^e_{\mathbf{k}})-\Theta(H-\xi^e_{\mathbf{k}})}{(\xi^e_{\mathbf{k}})^2}-\frac{\delta(H-\xi^e_{\mathbf{k}})+\delta(H+\xi^e_{\mathbf{k}})}{\xi^e_{\mathbf{k}}}\right],\\
\frac{\partial^2\Omega}{\partial M^2} &= \frac{m_0}{2GM}+2N_cM^2\sum_{e=\pm}\int^{\Lambda}\frac{d^3\mathbf{k}}{(2\pi)^3}\left[\frac{\Theta(H+\xi^e_{\mathbf{k}})-\Theta(H-\xi^e_{\mathbf{k}})}{E^3_{\mathbf{k}}}-\frac{\delta(H+\xi^e_{\mathbf{k}})+\delta(H-\xi^e_{\mathbf{k}})}{E^2_{\mathbf{k}}}\right].
\end{aligned} \tag{27}$$

The dynamical quark mass M in above expressions is self-consistently determined via the gap equation

$$\frac{\partial\Omega}{\partial M} = \frac{M-m_0}{2G} - 2N_cM\sum_{e=\pm}\int^{\Lambda}\frac{d^3\mathbf{k}}{(2\pi)^3}\frac{\Theta(H+\xi^e_{\mathbf{k}})-\Theta(H-\xi^e_{\mathbf{k}})}{E_{\mathbf{k}}} = 0. \tag{28}$$

While the expression of γ is not shown here, we have numerically checked that $\gamma > 0$ is always satisfied. Therefore the order of the phase transition depends only on the signs of α and β. A second-order phase transition requires that the α can change sign and $\beta > 0$ with respect to the control parameter(s) and $\alpha = 0$ at the critical point. The calculated results of the second-order phase transition line predicted by Ginzburg-Landau theory are shown in Fig. 4(a). It is apparent that such a result agrees well with that via minimizing $\Omega(M, \Delta)$. Notice that the condition $\alpha = 0$ is physically equivalent to the relation $\mu_I^c = m_\pi(\mu_I, H)$ where $m_\pi(\mu_I, H)$ is the in-medium pion mass. Here we find that the critical isospin chemical potential increases with the increasing of the baryon chemical potential or density, which is consistent with that observed in hadronic theories.

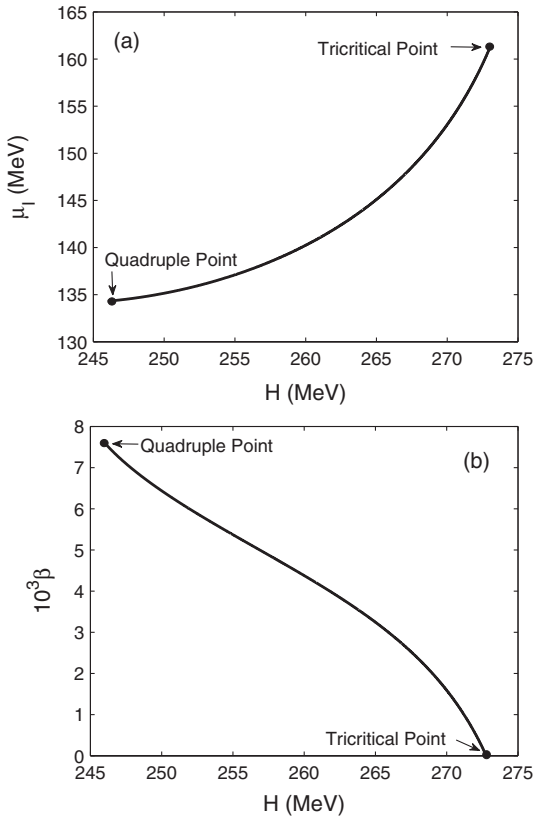

FIG. 4. (a) Calculated result of the second-order superfluid-normal phase boundary in Ginzburg-Landau theory. (b) The value of the coefficient β as a function of H along the second-order phase transition line.

When β changes its sign, the second-order phase transition turns to be first order, and the tricritical point $(\mu_I^{\rm tri}, \mu_B^{\rm tri})$ can be determined via the condition $\alpha = \beta = 0$. For our model parameter set we get $(\mu_I^{\rm tri}, H^{\rm tri}) = (160.5\ \text{MeV}, 272.8\ \text{MeV})$, which is in good agreement with the numerical results. Since the phase transition becomes of first order when $\mu_I > \mu_I^{\rm tri}$, the baryon matter with fixed baryon density ρ_B can be composed of normal baryon matter and pion condensed matter via phase equilibrium condition. Recall that the isospin chemical potential in neutron star matter can be as large as 200 MeV [40].

C. Gapless pion condensate and topological quantum phase transition

The most interesting phase in the phase diagram shown above is the gapless pion condensate, where the superfluid order parameter remains finite but the single-particle excitation in the lowest band becomes gapless. While we plot a line to separate the gapped and gapless phases, whether there is a phase transition in between remains a question since the symmetry of the order parameter does not change. In the following, we will identify the BEC-GPC transition as a topological quantum phase transition and determine the order of this phase transition.

First, we show the change in Fermi surface topology in the lowest quasiparticle band, similar to the Lifshitz transition in ordinary metals and quantum phase transition in non-s-wave fermion superfluids [41,42]. The zero temperature momentum distributions $n_{\mathrm{I,B}}(\mathbf{k})$ for quarks with quantum numbers (I, B) read [7]

$$
\begin{aligned}
n_{\pm 1/2,1/3}(\mathbf{k}) &= 1-\frac{1}{2}\Bigg[1+\frac{E_{\mathbf{k}}\mp\mu_{\mathrm{I}}/2}{\sqrt{(E_{\mathbf{k}}\mp\mu_{\mathrm{I}}/2)^2+\Delta^2}}\Bigg]\Theta(\sqrt{(E_{\mathbf{k}}\mp\mu_{\mathrm{I}}/2)^2+\Delta^2}-H),\\
n_{\pm 1/2,-1/3}(\mathbf{k}) &= \frac{1}{2}\Bigg[1-\frac{E_{\mathbf{k}}\mp\mu_{\mathrm{I}}/2}{\sqrt{(E_{\mathbf{k}}\mp\mu_{\mathrm{I}}/2)^2+\Delta^2}}\Bigg]\Theta(\sqrt{(E_{\mathbf{k}}\mp\mu_{\mathrm{I}}/2)^2+\Delta^2}-H).
\end{aligned}
\tag{29}
$$

In the gapped BEC phase we find that all momentum distributions are smooth. However, in the gapless phase, there forms a sharp Fermi surface at $|\mathbf{k}|=k_2$ in the distribution $n_{1/2,1/3}(\mathbf{k})$. More explicitly, in the gapless phase, $n_{1/2,1/3}(\mathbf{k})=1$ and $n_{1/2,-1/3}(\mathbf{k})=0$ for $|\mathbf{k}|<k_2$, and then jump to a smooth distribution when $|\mathbf{k}|>k_2$. In Fig. 5 we illustrate an example of the calculated results of the quasiparticle dispersion and the occupation number probability of the momentum state. Because of the appearance of a sharp gapless surface, the system generates a nonzero baryon density due to the full occupation of the quarks with (I, B) = (1/2, 1/3) inside the gapless surface. The critical mismatch H_c at which gapless single-particle excitation appears, then becomes a quantum critical point (QCP), and the system possesses different low-temperature thermodynamic behavior for the two sides $H<H_c$ and $H>H_c$. For example, the low-temperature specific heat C_V has an exponential behavior $C_V\propto e^{-\phi/T}$ at $H<H_c$, but becomes a linear function $C_V\propto T$ at $H>H_c$.

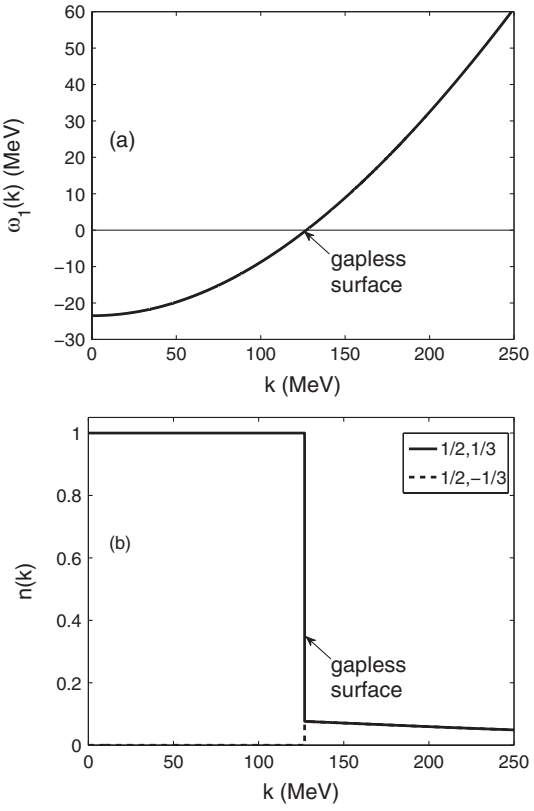

FIG. 5. Calculated results of the lowest single-particle excitation $\omega_1(\mathbf{k})$ (panel (a)) and the corresponding particle occupation numbers $n(\mathbf{k})$ (panel (b)), at $\mu_{\mathrm{I}}=150$ MeV and $H=265$ MeV. The numerical solutions for Δ and M are $\Delta=140.7$ MeV and $M=271.3$ MeV. The gapless surface is located at $k_2\simeq 127$ MeV.

Second, to identify a phase transition and determine its order we need to study the nonanalytical behavior of the thermodynamic potential at the QCP with $H=H_c$. (We assume μ_{I} keeps being fixed without loss of generality.) First, the quantum critical point with $H=H_c$ can be shown to be $H_c=\Delta_{\mathrm{ex}}(H=0)$. The argument is based on two folds: (1) The order parameter Δ and the dynamical quark mass M are single-value functions of H at least near the QCP. While this is hard to be proved, it is confirmed by our numerical results; (2) For $H<H_c$, there always exists solution $\Delta=\Delta_0$ and $M=M_0$. While, when $H>H_c$, it should be changed and hence the lowest band quasiparticle excitation becomes gapless. In Fig. 6(a) we display an example of the obtained variation behaviors of the superfluid order parameter Δ and the dynamical quark mass M with respect to the mismatch H. It shows evidently that the gapless phase starts at $H=\Delta_{\mathrm{ex}}$.

It is obvious that the thermodynamic potential in the gapped phase remains unchanged; then we have $d\Omega^n/dH^n=0$ when $H\rightarrow H_c^-$ for any integer n. Thus the nonanalytical behavior should be demonstrated by the value of $d\Omega^n/dH^n$ when $H\rightarrow H_c^+$. Keeping in mind here the order parameter $\Delta=\Delta(H)$ and the dynamical quark mass $M=M(H)$ are self-consistently determined as functions of H, taking the first derivative we obtain

$$
\begin{aligned}
f(H)\equiv\frac{d\Omega}{dH} &= \frac{\partial\Omega}{\partial H}+\frac{\partial\Omega}{\partial\Delta}\frac{d\Delta}{dH}+\frac{\partial\Omega}{\partial M}\frac{dM}{dH}\\
&= -\frac{N_c}{3\pi^2}\Bigg[\Bigg(\frac{\mu_{\mathrm{I}}}{2}+\sqrt{H^2-\Delta^2}\Bigg)^2-M^2\Bigg]^{3/2}.
\end{aligned}
\tag{30}
$$

Here we have made use of the saddle point condition $\partial\Omega/\partial\Delta=\partial\Omega/\partial M=0$. Taking the limit $H\rightarrow H_c^+$, we have $f(H)=0$. Thus the first derivative is continuous. The second derivative then reads

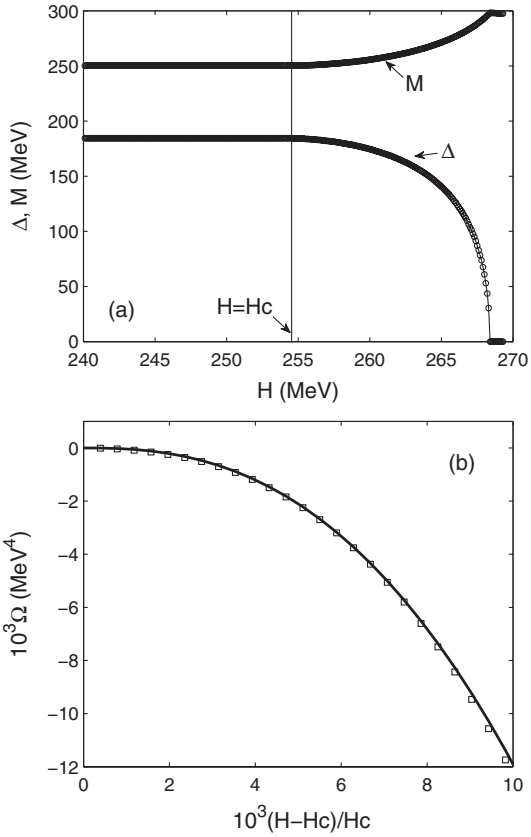

FIG. 6. (a) Calculated mismatch H dependence of the superfluid order parameter Δ and the dynamical quark mass M via minimizing the thermodynamic potential for given $\mu_I = 150$ MeV. The critical value of H at which the BEC-GPC phase transition takes place is $H_c = 254.4$ MeV. (b) Calculated variation behavior of the thermodynamic potential near the critical mismatch $H = H_c$. The square grids are the numerical data and the solid line is a power function $\propto (H - H_c)^{5/2}$.

$$g(H) \equiv \frac{d^2\Omega}{dH^2} = \frac{\partial f}{\partial H} + \frac{\partial f}{\partial \Delta}\frac{d\Delta}{dH} + \frac{\partial f}{\partial M}\frac{dM}{dH}. \tag{31}$$

Notice that we have to evaluate $d\Delta/dH$ and dM/dH since $\partial f/\partial\Delta$ and $\partial f/\partial M$ are no longer zero. They can be obtained from the stationary conditions. From $\partial\Omega/\partial\Delta = 0$ and $\partial\Omega/\partial M = 0$ we have

$$\begin{aligned} \frac{\partial}{\partial H}\frac{\partial\Omega}{\partial\Delta} + \frac{\partial^2\Omega}{\partial\Delta^2}\frac{d\Delta}{dH} + \frac{\partial^2\Omega}{\partial\Delta\partial M}\frac{dM}{dH} = 0, \\ \frac{\partial}{\partial H}\frac{\partial\Omega}{\partial M} + \frac{\partial^2\Omega}{\partial M^2}\frac{dM}{dH} + \frac{\partial^2\Omega}{\partial M\partial\Delta}\frac{d\Delta}{dH} = 0. \end{aligned} \tag{32}$$

Then we have

$$\begin{aligned} g(H) = \frac{\partial f}{\partial H} - \frac{1}{\det\mathcal{M}}\Bigg[\left(\frac{\partial f}{\partial\Delta}\right)^2\mathcal{M}_{11} \\ + \left(\frac{\partial f}{\partial M}\right)^2\mathcal{M}_{22} - 2\frac{\partial f}{\partial\Delta}\frac{\partial f}{\partial M}\mathcal{M}_{12}\Bigg], \end{aligned} \tag{33}$$

where $\mathcal{M}$ is the stability matrix

$$\mathcal{M} = \begin{pmatrix} \frac{\partial^2\Omega}{\partial M^2} & \frac{\partial^2\Omega}{\partial M\partial\Delta} \\ \frac{\partial^2\Omega}{\partial\Delta\partial M} & \frac{\partial^2\Omega}{\partial\Delta^2} \end{pmatrix}. \tag{34}$$

One can show that the second derivative is also continuous at the QCP. The proof is based on the following two folds: (1) The gapless phase is thermodynamically stable and hence there is no singularity in the matrix elements of $\mathcal{M}$ and also in $\det\mathcal{M}$; (2) The derivatives of $f(H)$ with respect to H, Δ, M are proportional to $[(\mu_I/2 + \sqrt{H^2 - \Delta^2})^2 - M^2]^{1/2}$. Thus we conclude that $g(H) \to 0$ when $H \to H_c^+$. Further, we observe that there develops a singularity in $d^3\Omega/dH^3$ since there is a singular term in $\partial^2 f/\partial H^2$ proportional to $[(\mu_I/2 + \sqrt{H^2 - \Delta^2})^2 - M^2]^{-1/2}$. Thus we find that $d^3\Omega/dH^3 \to \infty$ when $H \to H_c^+$, which means that there exists a third-order quantum phase transition at the QCP $H = H_c$.

In fact, the nonanalytical behavior near $H = H_c$ means that we can express the thermodynamic potential in the gapless phase as a power function

$$\Omega(H) - \Omega(H_c) = \kappa(H - H_c)^\nu, \qquad H \to H_c^+. \tag{35}$$

Since the phase transition is of third order, we should have $2 < \nu < 3$. In fact, employing a Taylor expansion near $H = H_c$ we can show that $f(H) \propto (H - H_c)^{3/2}$ providing that the changes in Δ, M are beyond the order $O(H - H_c)$. Thus we find $\nu = 5/2$, which is well consistent with our numerical results shown in Fig. 6(b). In condensed matter physics, such a kind of phase transition is also referred to as of second and half order [41].

The gapless phase studied here is free from not only the thermodynamic instability but also the so-called magnetic instability [22]. In our case, the magnetic instability is related to the response of the system to an external isospin current. The quantity which describes the response of the system to an external isospin current is the isospin current-current correlation tensor defined by

$$\Pi_3^{\mu\nu}(Q) = \frac{1}{2}\sum_K \mathrm{Tr}[\Gamma_3^\mu \mathcal{G}(K)\Gamma_3^\nu \mathcal{G}(K - Q)], \tag{36}$$

with $\Gamma_3^\mu = \tau_3\gamma^\mu/2$. We can define the superfluid density ρ_s in the long-wave and static limit as

$$\rho_s = \frac{1}{2}\lim_{\mathbf{q}\to 0}(\delta_{ij} - \hat{q}_i\hat{q}_j)\Pi_3^{ij}(\omega = 0, \mathbf{q}). \tag{37}$$

We have checked that in the whole gapless phase, the superfluid density keeps positive.

D. Chiral phase transition at small μ_I

Another interesting phase transition is the chiral phase transition located at small μ_I and large μ_B where the pion condensate vanishes. Hence we should analyze the following effective potential:

$$\Omega(M) = \frac{(M-m_0)^2}{4G} - 2N_c \int^{\Lambda} \frac{d^3\mathbf{k}}{(2\pi)^3}\left\{2E_{\mathbf{k}} + \sum_{i=u,d}[(E_{\mathbf{k}}-\mu_i)\Theta(\mu_i - E_{\mathbf{k}}) + (E_{\mathbf{k}}+\mu_i)\Theta(-\mu_i - E_{\mathbf{k}})]\right\}. \quad (38)$$

Since the current quark mass is nonzero, which breaks the chiral symmetry explicitly, the chiral phase transition can only be of first order or a smooth crossover. A first-order phase transition happens when the Nambu phase (with large M) and the Wigner phase (with smaller M) have the same potential [43]. To show the mismatch driven chiral phase transition clearly, we display in Fig. 7 the calculated variation behaviors of the effective quark mass M and the baryon density ρ_{B} with respect to the mismatch H at several isospin chemical potentials $\mu_{\mathrm{I}} < m_\pi$ with the commonly used parameters listed in Sec. II. The figure shows apparently that, at $\mu_{\mathrm{I}} = 0$, the first-order phase transition takes place at $H_\chi = 1.064M^*$ which is larger than the vacuum constituent quark mass. As a consequence, the system generates a nonzero baryon density at $H = M^*$ before the chiral phase transition. While this behavior may be unphysical due to the lack of confinement in the NJL model [44], the nature of the transition at $H = M^*$ can be shown to be the same as the BEC-GPC transition. Looking over Fig. 7 more carefully, one can recognize that a nonzero isospin chemical potential has two effects on the chiral phase transition: it reduces the critical baryon chemical potential and drives the transition to a smooth crossover. More concretely, at nonzero μ_{I}, the system generates a finite baryon density at $H = M^* - \mu_{\mathrm{I}}/2$. The first-order phase transition ends up at a critical isospin chemical potential $\mu_{\mathrm{I}} = 110$ MeV.

As pointed out by Buballa [36], the appearance of the low-density phase in the interval $M^* < H < H_\chi$ depends on model parameters. In our case discussed above, we have a relatively small vacuum constituent quark mass and hence $H_\chi > M^*$. To show the influence of the parameters, we take the model parameter set $m_0 = 5.6$ MeV, $\Lambda = 587.9$ MeV and $G\Lambda^2 = 2.44$ which has been used in Ref. [36]. The numerical results for $\mu_{\mathrm{I}} = 0$ and $\mu_{\mathrm{I}} = 100$ MeV are illustrated in Fig. 8. From the figure one can notice that, at $\mu_{\mathrm{I}} = 0$, the chiral phase transition takes place at $H_\chi = 0.955M^*$ and there is no low-density

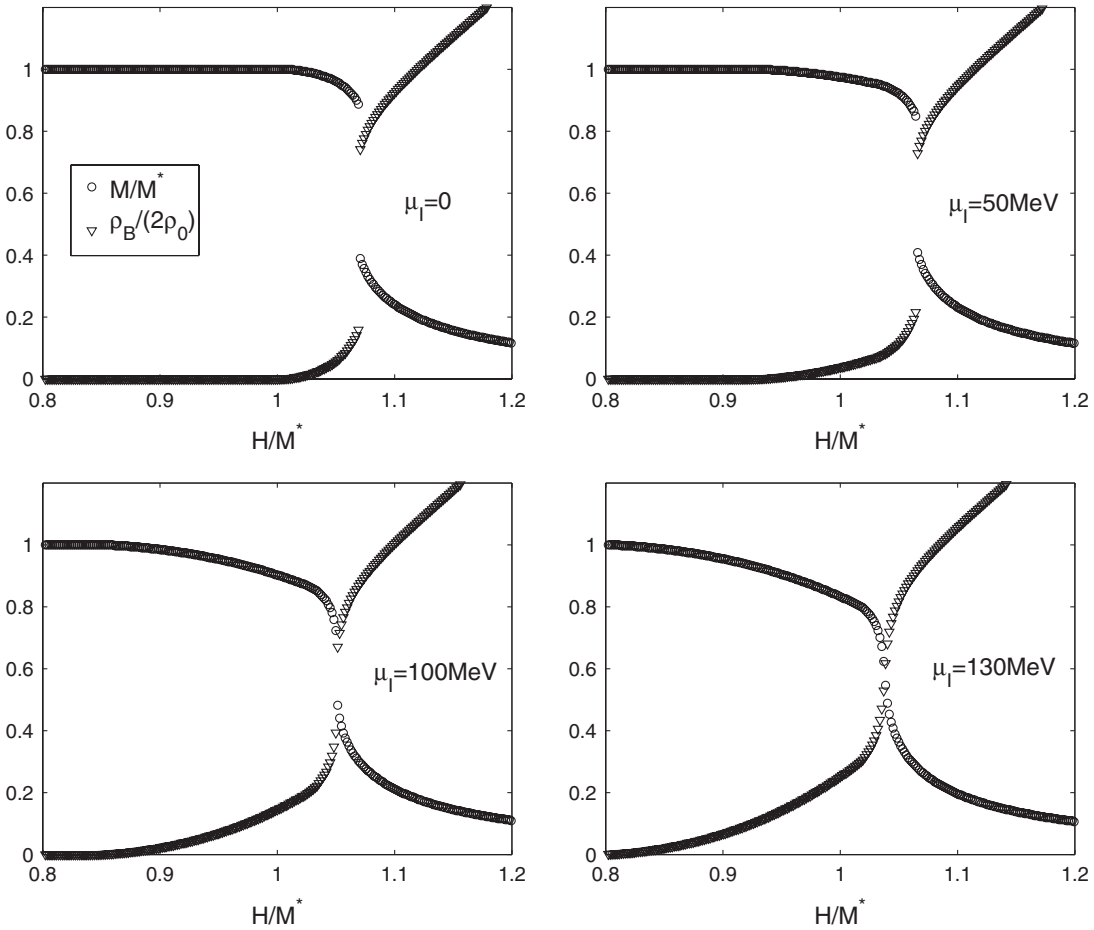

FIG. 7. Calculated results of the effective quark mass M (in unit M^*) and the baryon density ρ_{B} (in unit $2\rho_0$, where $\rho_0 = 0.17$ fm^{-3}) as functions of the mismatch H at several isospin chemical potentials $\mu_{\mathrm{I}} < m_\pi$.

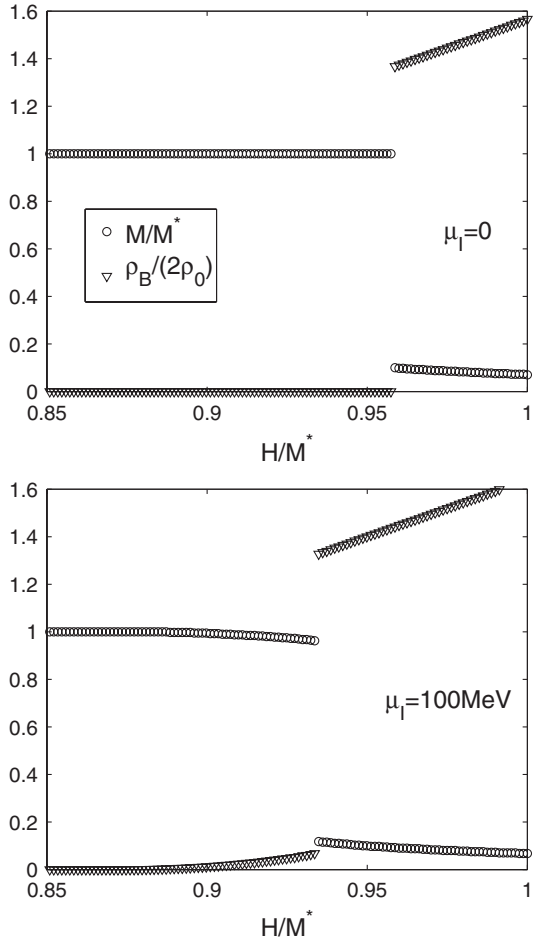

FIG. 8. Calculated results of the effective quark mass M (in unit M^*) and the baryon density ρ_B (in unit $2\rho_0$) as functions of the mismatch H with model parameter set $m_0 = 5.6$ MeV, $\Lambda = 587.9$ MeV, and $G\Lambda^2 = 2.44$ at several isospin chemical potentials.

interval. It provides evidence that, with a larger value of M^*, the low-density interval disappears. However, we also find that this phase can still appear in the presence of nonzero isospin chemical potential. This means that the quadruple point $(\mu_I, H) = (m_\pi, M^* - m_\pi/2)$ is not affected by a different model parameter set.

E. Comparison with cold atom system

In the final part of this section, we will point out that our $\mu_I - \mu_B$ phase diagram seems quite similar to that obtained in the investigation of BCS-BEC crossover in cold fermion systems. A typical phase diagram in the strongly interacting molecule region [26] is shown in Fig. 9. Here the molecule chemical potential μ_m and the effective Zeeman energy splitting h correspond to our isospin chemical potential μ_I and one third of the baryon chemical potential $H = \mu_B/3$, respectively. The SF phase corresponds to our pion condensed phase and SF_M is similar to our gapless pion condensate. One can easily find that the

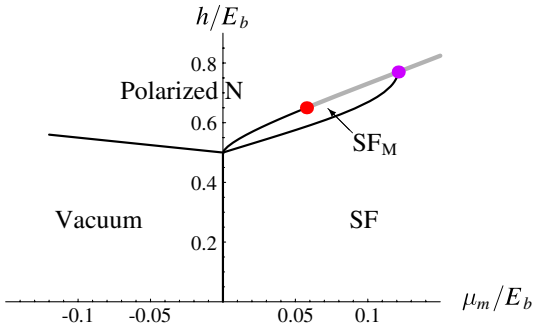

FIG. 9 (color online). The grand canonical $\mu_m - h$ phase diagram of a cold Fermi gas in the strong coupling molecule region (taken from Ref. [26]). The black and gray solid lines represent continuous and first-order phase transitions, respectively. Here E_b is the molecule binding energy, μ_m is the effective chemical potential of the molecules, and h is the Zeeman energy splitting. The molecule chemical potential μ_m is related to the fermion chemical potential μ by $\mu_m = 2\mu + E_b$.

topological structure of this phase diagram is the same as ours, except for the first-order chiral phase transition. However, the nature of the $SF - SF_M$ transition has not yet been well clarified in the cold atom scenario [25–28], and in some works it is stated that there exists no phase transition [28]. Such a transition, as we believe due to universality, is also a third-order quantum phase transition.

The quadruple point is universal if we define the pion binding energy as $E_b = 2M^* - m_\pi$ and a nonrelativistic chemical potential for pions as $\mu_m = \mu_I - m_\pi$. Then the quadruple point in our phase diagram is located at $(\mu_m/E_b, H/E_b) = (0, 0.5)$, which is the same as the phase diagram in Fig. 9. Furthermore, the tricritical point locating at $(\mu_m/E_b, H/E_b) = (0.054, 0.554)$ is also close to the cold atom phase diagram.

IV. PHASE STRUCTURE AT LARGE μ_I: LARKIN-OVCHINNIKOV-FULDE-FERRELL STATE

Beyond the BEC region, we find that the phase transition from the superfluid phase to the normal phase is always of first order, like the behavior of BCS superconductors in a Zeeman field. There arises then an interesting problem whether some unconventional superfluid state with smaller superfluid order parameter Δ can exist above the first-order phase transition line. This leads to the famous idea of an inhomogeneous Larkin-Ovchinnikov-Fulde-Ferrell (LOFF) state [18,19]. In this state, the Cooper pairs condense with a nonzero total momentum and the superfluid order parameter oscillates in coordinate space.

In our case it is possible to consider the version proposed by Fulde and Ferrell where the phase of order parameter varies with coordinates [18]. Considering the fact that the order parameter fields π_+ and π_- are indeed complex conjugates to each other, we take the following single-plane-wave ansatz

$$\langle\Phi\rangle = -4G\langle\bar{u}i\gamma_5 d\rangle = \Delta e^{2i\mathbf{q}\cdot\mathbf{r}},$$
$$\langle\Phi^*\rangle = -4G\langle\bar{d}i\gamma_5 u\rangle = \Delta e^{-2i\mathbf{q}\cdot\mathbf{r}}. \tag{39}$$

Transforming to π_1 and π_2 fields, we find

$$\langle\pi_1\rangle = \Delta\cos(2\mathbf{q}\cdot\mathbf{r}), \qquad \langle\pi_2\rangle = \Delta\sin(2\mathbf{q}\cdot\mathbf{r}), \tag{40}$$

which recovers the original idea of pion condensation that pions condense with nonzero momentum [40]. However, if such a possibility with $\mathbf{q} \neq 0$ occurs at large μ_I, it is unlike the case suggested in Ref. [40] where pions remain tightly bound objects. In our model it has been found that pions condense in a gapless state with zero momentum at finite baryon density. On the other hand, one may consider more complicated Ansätze proposed by Larkin and Ovchinnikov [19], in which the order parameter forms a one-dimensional standing wave with nodal planes spaced by $\pi/(2|\mathbf{q}|)$. While the multiple plane wave state is generally more favored than the single wave state [45], the single-plane-wave FF Ansatz is enough for us to analyze the phase structure at large μ_I.

It is not easy to evaluate the effective potential for general Ansätze, but in our case, it can be calculated through a phase transformation for the two quark flavors,

$$\chi_u(\tau,\mathbf{r}) = u(\tau,\mathbf{r})e^{-i\mathbf{q}\cdot\mathbf{r}},$$
$$\chi_d(\tau,\mathbf{r}) = d(\tau,\mathbf{r})e^{i\mathbf{q}\cdot\mathbf{r}}. \tag{41}$$

It is evident that the measure of the path integral is not changed, and the coordinate-dependence of the order parameter is totally removed. Then the thermodynamic potential can be expressed as

$$\Omega(M,\Delta,\mathbf{q}) = \frac{(M-m_0)^2+\Delta^2}{4G} - \frac{T}{V}\ln\det\mathcal{G}^{-1}(K,\mathbf{q}), \tag{42}$$

where the inverse quark propagator reads

$$\mathcal{G}^{-1}(K,\mathbf{q}) = \begin{pmatrix} \gamma^\mu K_\mu - \boldsymbol{\gamma}\cdot\mathbf{q} + \mu_u\gamma_0 - M & -i\gamma_5\Delta \\ -i\gamma_5\Delta & \gamma^\mu K_\mu + \boldsymbol{\gamma}\cdot\mathbf{q} + \mu_d\gamma_0 - M \end{pmatrix}. \tag{43}$$

A. Phase diagram: Numerical results

The thermodynamic potential $\Omega(M,\Delta,\mathbf{q})$ can be evaluated with the result

$$[\det\mathcal{G}^{-1}]^{1/2} = [(i\omega_n + H + E_-)^2 - (E_+ - \mu_I/2)^2 - \Delta^2][(i\omega_n + H - E_-)^2 - (E_+ + \mu_I/2)^2 - \Delta^2] + 2\Delta^2(E_{\mathbf{k}}^2 - E_{\mathbf{k}+\mathbf{q}}E_{\mathbf{k}-\mathbf{q}} - \mathbf{q}^2) \tag{44}$$

where $E_\pm = (E_{\mathbf{k}+\mathbf{q}} \pm E_{\mathbf{k}-\mathbf{q}})/2$. It is evident that the last term vanishes when $|\mathbf{q}| = 0$ and can be neglected since Δ is relatively small in the LOFF state [18,19,45]. Then the thermodynamic potential at $T = 0$ reads

$$\begin{aligned}\Omega(M,\Delta,\mathbf{q}) = {} & \frac{(M-m_0)^2+\Delta^2}{4G} - 2N_c\int^\Lambda\frac{d^3\mathbf{k}}{(2\pi)^3}\left[\sqrt{\left(E_+ - \frac{\mu_I}{2}\right)^2+\Delta^2} + \sqrt{\left(E_+ + \frac{\mu_I}{2}\right)^2+\Delta^2}\right] \\ & + 2N_c\int^\Lambda\frac{d^3\mathbf{k}}{(2\pi)^3}\left(\sqrt{\left(E_+ - \frac{\mu_I}{2}\right)^2+\Delta^2} - H - E_-\right)\Theta\left(H + E_- - \sqrt{\left(E_+ - \frac{\mu_I}{2}\right)^2+\Delta^2}\right) \\ & + 2N_c\int^\Lambda\frac{d^3\mathbf{k}}{(2\pi)^3}\left(\sqrt{\left(E_+ - \frac{\mu_I}{2}\right)^2+\Delta^2} + H + E_-\right)\Theta\left(-H - E_- - \sqrt{\left(E_+ - \frac{\mu_I}{2}\right)^2+\Delta^2}\right) \\ & + 2N_c\int^\Lambda\frac{d^3\mathbf{k}}{(2\pi)^3}\left(\sqrt{\left(E_+ + \frac{\mu_I}{2}\right)^2+\Delta^2} - H + E_-\right)\Theta\left(H - E_- - \sqrt{\left(E_+ + \frac{\mu_I}{2}\right)^2+\Delta^2}\right) \\ & + 2N_c\int^\Lambda\frac{d^3\mathbf{k}}{(2\pi)^3}\left(\sqrt{\left(E_+ + \frac{\mu_I}{2}\right)^2+\Delta^2} + H - E_-\right)\Theta\left(-H + E_- - \sqrt{\left(E_+ + \frac{\mu_I}{2}\right)^2+\Delta^2}\right).\end{aligned} \tag{45}$$

When $\Delta = 0$, the thermodynamic potential $\Omega(M,0,\mathbf{q})$ should recover the case of free quark gas with mass M in the mean field approach. However, due to the presence of a cutoff Λ for the three-dimensional integral in this non-renormalizable model, the thermodynamic potential includes an unphysical term proportional to $-\mathbf{q}^2\Lambda^2$ which

should be subtracted. Such a subtraction corresponds physically to a vanishing superfluid density ρ_s in the normal phase with $\Delta = 0$, since we have the relation $\rho_s = \partial^2\Omega/\partial q^2|_{q=0}$ [9]. The unphysical term occurs in fact in any relativistic approach with three-dimensional cutoff due to its removing of the spatial asymmetry of the related quasiparticle spectrum. Within a nonrelativistic theory one can remove all divergences once the coupling is renormalized (details can be seen in the appendix of Ref. [46]). For relativistic systems, various regularization schemes have been implemented to avoid the unphysical term related with the three-momentum cutoff Λ [47,48]. However, the thermodynamic potential remains logarithmically divergent even after the combination of the Pauli-Villars regularization and the proper-time regularization; one has to then subtract the remaining divergency by calculating the difference to some reference point, like the ground state in vacuum or simply a normal conducting phase at some given chemical potential [47]. The dimensional regularization has also been applied to high-density quark matter in the NJL model [48]. To our knowledge, no work has been done to discuss the LOFF phase in the framework of the NJL model with dimensional regularization. The difference between different regularization schemes for such a system has not yet been investigated either. However, they should agree with each other qualitatively from Nickel and Buballa's result [47]. Here we follow then Fukushima and Iida's practical treatment [49]. First we minimize the thermodynamic potential with respect to M and Δ to obtain the optimal value $M(\mathbf{q})$ and $\Delta(\mathbf{q})$ as functions of $\mathbf{q}$, because the explicit forms of the gap equations for M and Δ are not affected by this unphysical term. Only the gap equation for $\mathbf{q}$ is modified. We then extract the unphysical term and define the physical thermodynamic potential as

$$\Omega_{\rm sub}(T, \mu_{\rm I}, \mu_{\rm B}, \mathbf{q}) = \Omega(T, \mu_{\rm I}, \mu_{\rm B}, \mathbf{q}, M(\mathbf{q}), \Delta(\mathbf{q})) - \Omega(T, \mu_{\rm I}, \mu_{\rm B}, \mathbf{q}, M(\mathbf{q}), \Delta(\mathbf{q}) = 0). \tag{46}$$

The optimal value of $\mathbf{q}$ is obtained via minimizing $\Omega_{\rm sub}(T, \mu_{\rm I}, \mu_{\rm B}, \mathbf{q})$ with respect to q. Notice that the thermodynamic potential is only a function of $q \equiv |\mathbf{q}|$, which means that the direction of $\mathbf{q}$ is spontaneously generated and we need to minimize $\Omega_{\rm sub}$ only with respect to q. Another subtraction procedure was recently proposed by Andersen and Brauner [46]. The final expression for the subtracted thermodynamic potential in their prescription reads

$$\Omega_{\rm sub}(M, \Delta, q) = \Omega(M, \Delta, q) - \Omega(M, 0, q) + \Omega(M, 0, 0). \tag{47}$$

The physical values of M, Δ and q can be obtained via minimizing $\Omega_{\rm sub}(M, \Delta, q)$ with respect to M, Δ, q simultaneously. In this prescription, the thermodynamic potential is both well defined and physically consistent with the case of $q = 0$ studied in Sec. III. However, since the effective quark mass M is relatively small in the LOFF phase, the numerical results from the two prescriptions may be slightly different. In this work, we adopt the former prescription.

The calculated result of the phase diagram including the LOFF phase at large $\mu_{\rm I}$ is shown in Fig. 10. In a wide region of $\mu_{\rm I}$, the superfluid phase and the normal phase are separated by a first-order phase transition line, and the LOFF phase appears at a critical point $(\mu_{\rm I}, H) = (6.36m_\pi, 0.71M^*)$. Since the LOFF phase is favored only for large $\mu_{\rm I}$, our discussion in Secs. II and III including only $\mathbf{q} = 0$ ansatz is correct. In the region $\mu_{\rm I} > 6.36m_\pi$, the homogeneous superfluid phase undergoes a first-order phase transition to the LOFF state with a smaller order parameter Δ at some certain value of mismatch H (also the baryon chemical potential since $H = \mu_{\rm B}/N_c$). For a rough estimation, we find that, at the onset of the LOFF phase, $\Delta_{\rm LOFF} \sim 0.3\Delta_0$, thus we have $(\Delta_{\rm LOFF}/\Delta_0)^2 \sim 0.1$ and the approximation we employed to evaluate the thermodynamic potential is safe. At higher H, the LOFF phase undergoes a second-order phase transition to the normal phase. A similar phase diagram has been found in two-color quark matter [46,49]. It seems naïve that the result for the LOFF state to appear at so high an isospin chemical potential is not reliable or solid enough, since the critical one $\mu_{\rm I} > 6.36m_\pi \sim 880$ MeV is larger than the cutoff $\Lambda = 650$ MeV of the integral. In fact, according to

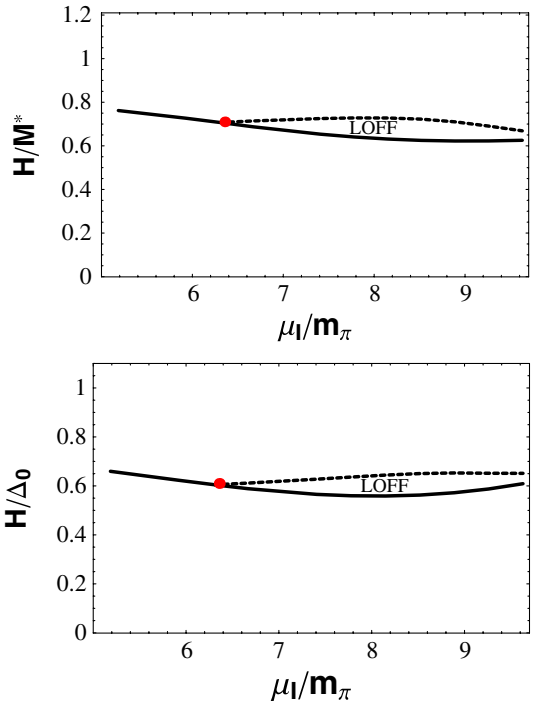

FIG. 10 (color online). Calculated results of the $\mu_{\rm I} - H$ phase diagram at large isospin chemical potential. The vertical axis is scaled by effective quark mass M^* in vacuum and the BCS gap Δ_0 at $H = 0$ for the upper and lower panels, respectively.

Eq. (3), the chemical potential of $\bar{d}$ quark is $\mu_{\bar{d}} = -\mu_B/N_c + \mu_I/2$. We can see then that $\mu_I/2$ (but not μ_I) embodies the mean Fermi surface of u and $\bar{d}$ quarks. Such a value of the mean Fermi energy ($\mu_I/2$) is apparently less than the three-momentum cutoff Λ, so that the calculation is meaningful. Therefore our present result for the LOFF phase to appear at very large isospin chemical potential is valid and reliable.

The LOFF window in terms of the BCS gap Δ_0 is significantly different from that in the weak coupling case, i.e., $0.707\Delta_0 < H < 0.754\Delta_0$. This means that the superfluid state at $\mu_I \sim (6-10)m_\pi$ is still in the strong coupling region. The LOFF window will be closed at large enough μ_I, which should be an artificial and unrealistic phenomenon due to the use of a hard cutoff in the NJL model. At asymptotic chemical potential, perturbative QCD calculation is available. The BCS gap at leading order can be expressed as [4]

$$\Delta_0 = bg^{-5}\frac{\mu_I}{2}\exp\left(-\frac{3\pi^2}{2g}\right), \tag{48}$$

where $b = 512\pi^4 \sim 10^4$ and $g = g(\mu_I/2)$ is the QCD running coupling constant. Implementing the two-loop approximation for the running coupling g, we can estimate that the BCS gap at $\mu_I = 9m_\pi$ is in the range 450–700 MeV for $\Lambda_{QCD} = (200\text{–}400)$ MeV. Even though the perturbative calculation fails at nonasymptotic density, we believe that the LOFF phase here should be continued with that at asymptotic density [4], where the LOFF window is identical to the weak coupling case $0.707\Delta_0 < H < 0.754\Delta_0$.

To analyze the stability of the LOFF state, we have calculated the thermodynamic potential in terms of the order parameter Δ and the momentum q. The obtained result of the contour plot of the thermodynamic potential on the $\Delta - q$ plane is displayed in Fig. 11. Our calculation manifests that the LOFF state, which has a small value of Δ and a large value of q, is located at the real global minimum. It indicates that the LOFF state is stable. Meanwhile, there also arises a gapless pion condensed phase which is at a maximum in both Δ and q directions. This isotropic gapless phase, which has two gapless surfaces $|\mathbf{k}| = k_1$ and $|\mathbf{k}| = k_2$ and is similar to that found in color superconductivity [21], is then an unstable solution in the BCS region. Note that the size of the LOFF momentum q in the whole LOFF phase is of order 300 MeV, It implies that the LOFF state at $\mu_I \sim 1$ GeV is not like the weak coupling case.

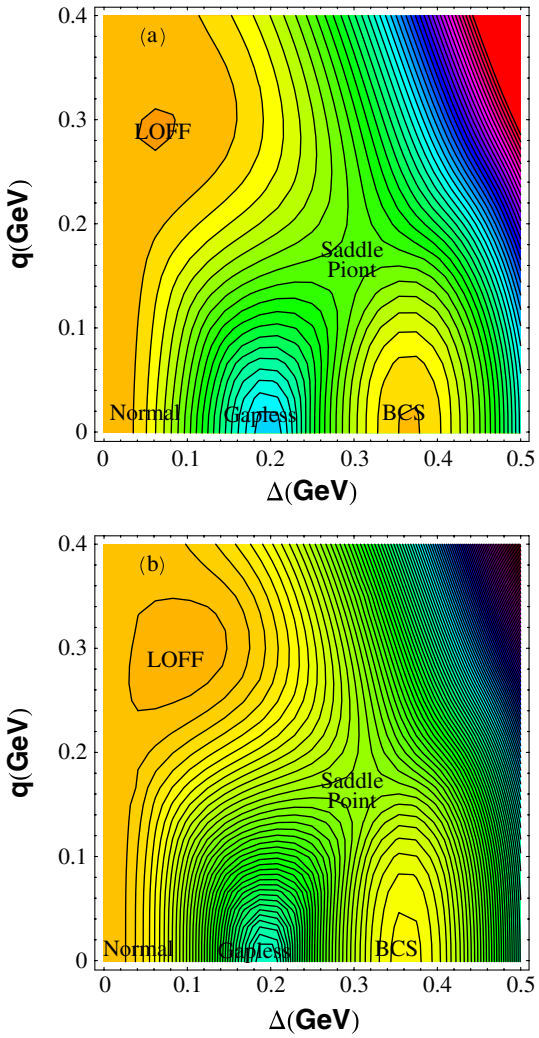

FIG. 11 (color online). Calculated results of the contour plots of the thermodynamic potential Ω_{sub} in the $\Delta - q$ plane at different conditions. Panel (a) at $\mu_I = 900$ MeV and $H = 217$ MeV, panel (b) at $\mu_I = 1000$ MeV and $H = 210$ MeV. In both cases, the LOFF solution is the global minimum.

B. Anisotropic quasiparticles and particle momentum distributions

The spontaneous generation of a nonzero Cooper pair momentum $2\mathbf{q}$ breaks the rotational symmetry $O(3)$ down to $O(2)$. Taking the approximation we employed for Eq. (45), we can get the quark's Green's function and in turn obtain the single-particle excitation spectrum via analyzing the localization of the poles. The result can be written as

$$\begin{aligned}
\omega_1(\mathbf{k}) &= \sqrt{\left(E_+ - \frac{\mu_I}{2}\right)^2 + \Delta^2} - (H + E_-),\\
\omega_2(\mathbf{k}) &= -\sqrt{\left(E_+ - \frac{\mu_I}{2}\right)^2 + \Delta^2} - (H + E_-),\\
\omega_3(\mathbf{k}) &= \sqrt{\left(E_+ + \frac{\mu_I}{2}\right)^2 + \Delta^2} - (H - E_-),\\
\omega_4(\mathbf{k}) &= -\sqrt{\left(E_+ + \frac{\mu_I}{2}\right)^2 + \Delta^2} - (H - E_-).
\end{aligned} \tag{49}$$

The anisotropic quasiparticles carry nonzero current, which can cancel the current carried by the condensate at

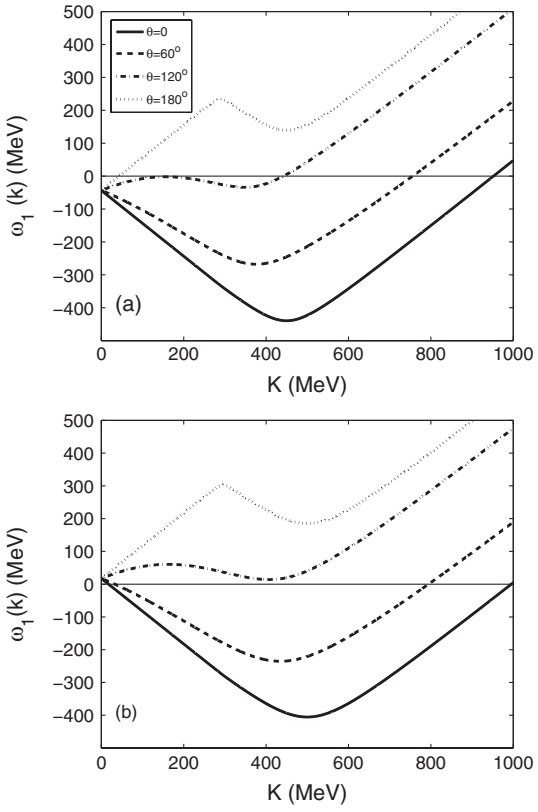

FIG. 12. Calculated results of the dispersion relation for the quasiparticle branch $\omega_1(\mathbf{k})$ at several cases of the angle θ. Panel (a) for the case with $\mu_I = 900$ MeV and $H = 217$ MeV, panel (b) for $\mu_I = 1000$ MeV and $H = 210$ MeV.

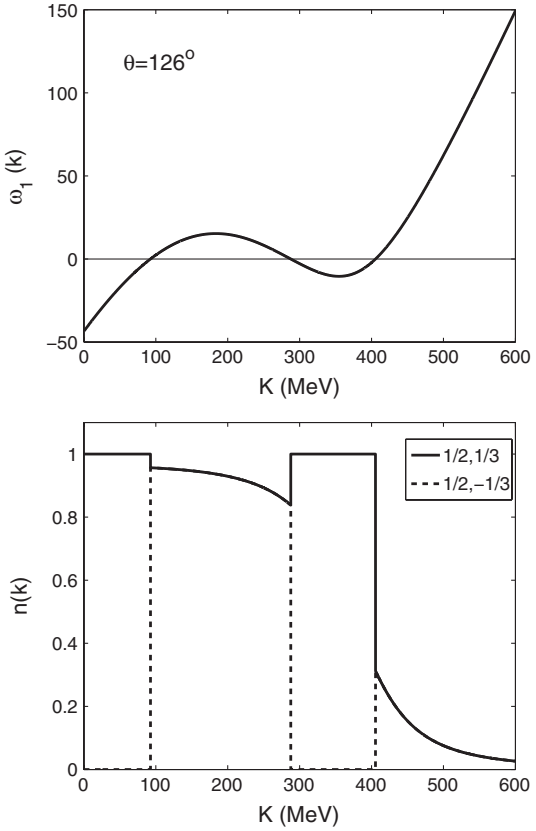

FIG. 13. An example of the calculated dispersion relation for the quasiparticle branch $\omega_1(\mathbf{k})$ and the corresponding particle momentum distributions $n(\mathbf{k})$ at $\theta = 126^o$, and with $\mu_I = 900$ MeV and $H = 217$ MeV.

the minimum $q = q_{\mathrm{LOFF}}$ and ensures that the total current in the ground state is zero. At large μ_I and small M, only the lowest band ω_1 is relevant for our discussion.

In Fig. 12, we illustrate the calculated results of the dispersion of the lowest band excitation $\omega_1(\mathbf{k})$ for several values of the angle θ between $\mathbf{k}$ and the LOFF momentum $\mathbf{q}$. It is apparent that the dispersions, which are indeed anisotropic, are distinct to the weak coupling case [18,45]. In the weak coupling case, we have $|\mathbf{q}| \ll k_F \simeq \mu_I/2$, and the quasiparticle dispersions $\omega_{1,2}$ can be approximated as

$$\omega_{1,2}(\mathbf{k}) = \pm\sqrt{\left(E_{\mathbf{k}} - \frac{\mu_I}{2}\right)^2 + \Delta^2} - (H + q\cos\theta). \quad (50)$$

Hence the quasiparticles can have two gapless nodes in a wide range of θ and the Fermi surface topology is the same as that of the conventional FF state [18]. However, for the strong coupling case here, since the value of $|\mathbf{q}|$ can be compared with $\mu_I/2$, we have the possibility to have one or three gapless nodes, which make the Fermi surface topology quite different to the weak coupling case. Analytically, we find this happens when $\omega_1(\mathbf{0}) < 0$, i.e.,

$$\sqrt{\left(\sqrt{\mathbf{q}^2 + M^2} - \frac{\mu_I}{2}\right)^2 + \Delta^2} < H. \quad (51)$$

Since M is quite small in the LOFF phase, this condition can be satisfied only when $|\mathbf{q}| \sim \mu_I/2$. In Fig. 13, we show a numerical sample of the quasiparticle's dispersion $\omega_1(\mathbf{k})$ which has three gapless nodes. The corresponding particle momentum distribution can be obtained from Eq. (29) via the replacement $E_{\mathbf{k}} \to E_+$ and $H \to H + E_-$ and is also shown in Fig. 13. Corresponding to the three gapless nodes, we have two blocking regions where one species is occupied and the other one is empty. We expect this phenomenon to appear also in the LOFF state of two-color quark matter [46,49]. Since the Fermi surface topology is different from that of the conventional FF pairing, there may exist topological quantum phase transition between different FF states. We defer this investigation to future work.

V. CHARGED PION MODES IN THE NORMAL PHASE

In Sec. II we once mentioned that there may exist charged pion modes in the normal phase. We discuss

now the properties of the charged pion modes in the normal phase with $\Delta = 0$ in some detail. In the finite temperature case, the pion spectral function has a characteristic change when the system undergoes a BEC-BCS crossover [10]: above the critical temperature $T_c(\mu_I)$, pions are tightly bound states in the BEC region $\mu_I < \mu_I^0 \simeq 230$ MeV, however, they become unstable resonances beyond the BEC region. Here we will show that the effect of finite baryon chemical potential or mismatch H is quite different from that of temperature.

The in-medium propagator of charged pions can be evaluated as

$$\mathcal{D}(i\nu_m, \mathbf{q}) = \frac{2G}{1 - 2G\Pi(i\nu_m, \mathbf{q})}, \tag{52}$$

where $\Pi(i\nu_m, \mathbf{q})$ is the polarization function for charged pions, and reads

$$\Pi(i\nu_m, \mathbf{q}) = 2N_c \sum_m \int \frac{d^3\mathbf{k}}{(2\pi)^3} \mathrm{Tr}[\mathcal{G}_u(i\omega_n, \mathbf{k}) i\gamma_5 \mathcal{G}_d(i\omega_n + i\nu_m, \mathbf{k} + \mathbf{q}) i\gamma_5]. \tag{53}$$

Here $\nu_m = 2\pi m T$ is the boson's Matsubara frequency, and $\mathcal{G}_i(i\omega_n, \mathbf{k}) = (i\omega_n + \mu_i)\gamma_0 - \boldsymbol{\gamma}\cdot\mathbf{k} (i = u, d)$ is the Green's function for the two quark flavors. Then the spectral function of charged pions can be defined as

$$\rho(\omega, \mathbf{q}) = -2\,\mathrm{Im}\mathcal{D}_R(\omega, \mathbf{q}) = \frac{-2\,\mathrm{Im}\Pi_R(\omega, \mathbf{q})}{[1/(2G) - \mathrm{Re}\Pi_R(\omega, \mathbf{q})]^2 + [\mathrm{Im}\Pi_R(\omega, \mathbf{q})]^2}, \tag{54}$$

where $X_R(\omega, \mathbf{q}) \equiv X(\omega + i\eta, \mathbf{q})$ is the analytical continuation of the function $X(i\nu_m, \mathbf{q})$. At zero pion momentum $\mathbf{q} = 0$, the real and the imaginary parts of $\Pi_R(\omega, \mathbf{q})$ can be evaluated as

$$\begin{aligned}
\mathrm{Re}\Pi_R(\omega, \mathbf{0}) &= 4N_c \int \frac{d^3\mathbf{k}}{(2\pi)^3} \left[\frac{1 - f(\xi_\mathbf{k}^- + H) - f(\xi_\mathbf{k}^- - H)}{2\xi_\mathbf{k}^- - \omega} + \frac{1 - f(\xi_\mathbf{k}^+ + H) - f(\xi_\mathbf{k}^+ - H)}{2\xi_\mathbf{k}^+ + \omega} \right], \\
\mathrm{Im}\Pi_R(\omega, \mathbf{0}) &= \frac{N_c}{4\pi} |\omega + \mu_I| \sqrt{(\omega + \mu_I)^2 - 4M^2} [1 - f(\omega/2 + H) - f(\omega/2 - H)] \\
&\quad \times [\Theta(\omega + \mu_I - 2M) + \Theta(-\omega - \mu_I - 2M)],
\end{aligned} \tag{55}$$

where $f(x) = 1/(e^{x/T} + 1)$ is the Fermi-Dirac distribution function.

Now we can see clearly the difference between the effect of finite temperature and that of finite baryon chemical potential. Here since we consider the $\mu_I > 0$ case and the relevant mode is π^+; let us focus on the $\omega > 0$ region. At $H = 0$ and $T > T_c$, the threshold for the decay process $\pi^+ \to \bar{q}q$ is $\omega_{\mathrm{th}} = 2M - \mu_I$. The bound states become unstable when the solution of the pole equation $1/(2G) - \mathrm{Re}\Pi_R(\omega, \mathbf{0}) = 0$ approaches the threshold frequency ω_{th}. It has been shown in Ref. [10] that pions are bound states above T_c in the BEC region with $\mu_I < \mu_I^0$, while they becomes unstable resonances beyond the BEC region. However, for the case $T = 0$ and $H > H_{\mathrm{Normal}}$, the threshold becomes

$$\omega_{\mathrm{th}} = \max\{2M - \mu_I, 2H\}, \tag{56}$$

since at $T = 0$ we have $1 - f(\omega/2 + H) - f(\omega/2 - H) = \Theta(2H + \omega) - \Theta(2H - \omega)$. Thus charged pions can still be in bound states even beyond the BEC region where $\mu_I > \mu_I^0$. The physical picture is clear: for π^+ mode, the decay process is $\pi^+ \to u\bar{d}$. At sufficiently low μ_I, namely $\mu_I/2 - H < M$, the Fermi surface for u quarks is formed while the one for anti-d quarks is not formed. Thus the decay process $\pi^+ \to u\bar{d}$ is greatly suppressed due to the lack of an anti-d quark channel in the medium. The equation $\mu_I/2 - H = M(\mu_I, H)$ then separates the normal phase with two regions, one with Fermi surfaces only for quarks and the other with a Fermi surface with anti-d quarks, as shown in the lower panel of Fig. 1 by a dot-dashed line. Obviously, this is a quantum phase transition between the two normal phases since the appearance of a new Fermi surface.

In Fig. 14 we show the calculated spectral function $\rho(\omega, \mathbf{0})$ above the superfluid-normal transition line for different isospin chemical potentials. It is clear that the π^+ mode is a bound state even at large isospin chemical potential, since the decay threshold becomes $\omega_{\mathrm{th}} = 2H$ in a wide range of μ_I. The bound state disappears when the solution of the pole equation, $\omega = \omega_{\mathrm{pole}}$, becomes larger than ω_{th}. Numerically, we find that this happens at $\mu_I \simeq 6.34 m_\pi$, which is very close to the onset of the isospin chemical potential for the LOFF phase. This is similar to the observation in cold atoms that the LOFF phase appears only at the BCS side [26]. Thus the disappearance of the π^+ bound state and the appearance of the LOFF phase gives a rough estimation of the BCS region. It means that the system is in the so-called crossover region for $\mu_I \in (1.67 m_\pi, 6.34 m_\pi)$. In conclusion, the behavior of the charged pion modes in the normal phase at large H is quite

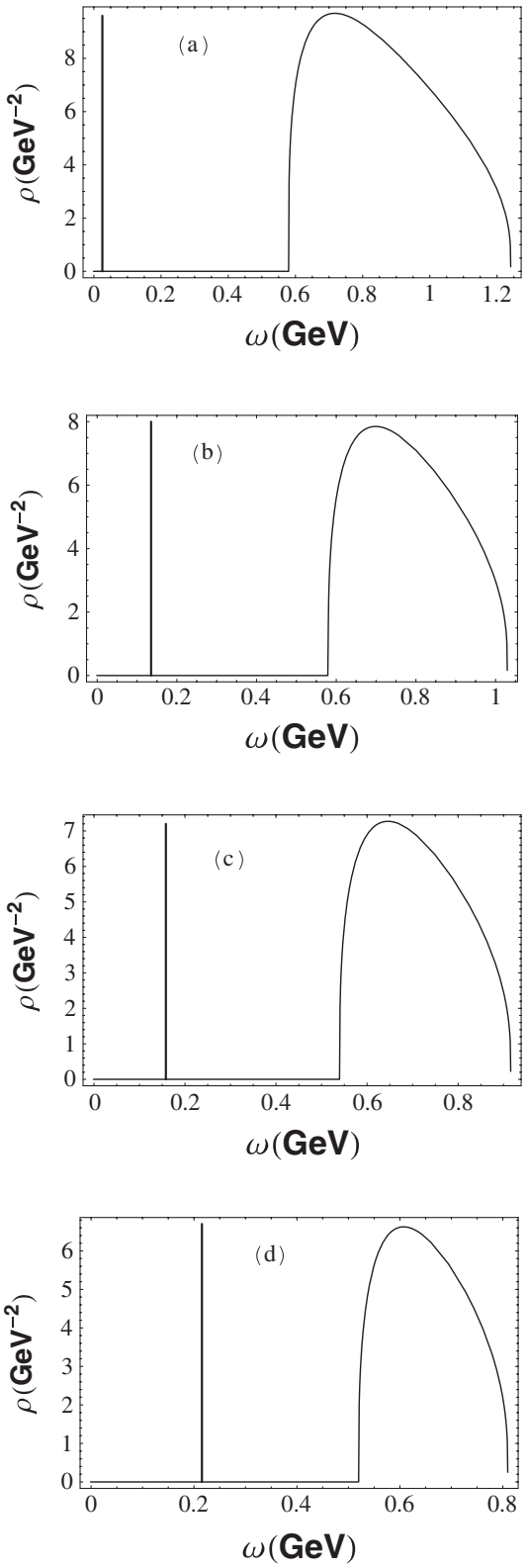

FIG. 14. Calculated spectral function $\rho(\omega, \mathbf{0})$ above the superfluid-normal transition line $H_{\mathrm{Normal}}(\mu_{\mathrm{I}})$ for several isospin chemical potentials (panels (a)-(d) are: (a) for $\mu_{\mathrm{I}} = 170$ MeV, $H = 290$ MeV, (b) for $\mu_{\mathrm{I}} = 300$ MeV, $H = 290$ MeV, (c) for $\mu_{\mathrm{I}} = 400$ MeV, $H = 270$ MeV, and (d) for $\mu_{\mathrm{I}} = 500$ MeV, $H = 260$ MeV.)

different from that above T_c, which gives a rough estimation of the boundary of the BCS and crossover regions. Such a result is quite similar to that which has been found in the normal phase of imbalanced Fermi gases [50].

VI. SUMMARY

In summary, we have investigated the phase diagram of QCD in terms of the isospin chemical potential and the baryon chemical potential (i.e., in the $\mu_{\mathrm{I}} - \mu_{\mathrm{B}}$ plane) in the microscopic Nambu–Jona-Lasinio model. The $\mu_{\mathrm{I}} - \mu_{\mathrm{B}}$ phase diagram shows a rich phase structure since the system undergoes a crossover from a Bose-Einstein condensate of charged pions to a BCS superfluid with condensed quark-antiquark Cooper pairs when μ_{I} increases at $\mu_{\mathrm{B}} = 0$. The isospin chemical potential μ_{I} serves as a parameter for the BEC-BCS crossover and the baryon chemical potential μ_{B} behaves as an effective mismatch between the pairing species. Thus the phase diagram is similar to that found in imbalanced Fermi gases, if the phase diagrams of BEC-BCS crossover in imbalanced systems are universal. We indeed found a similar phase diagram in the $\mu_{\mathrm{I}} - \mu_{\mathrm{B}}$ plane. A gapless pion condensed phase appears near the quadruple point $(\mu_{\mathrm{I}}, \mu_{\mathrm{B}}) = (m_\pi, M_{\mathrm{N}} - 1.5m_\pi)$ and ceases to exist beyond the BEC region. In contrast to those statements in some literature, we found that there is a third-order (or second- and half-order) quantum phase transition between the gapped and gapless phases. At very large isospin chemical potential, $\mu_{\mathrm{I}} > 6.36m_\pi$, an inhomogeneous LOFF superfluid phase appears in a window of μ_{B}, which should in principle exist for arbitrary large μ_{I}. Between the gapless and LOFF phases, the pion superfluid phase and the normal quark matter phase are connected by a simple first-order phase transition. QCD at finite isospin density and the $\mu_{\mathrm{I}} - \mu_{\mathrm{B}}$ phase diagram provide then concrete examples of BEC-BCS crossover with and without mismatch.

ACKNOWLEDGMENTS

The authors are highly grateful to Professor Dr. Jens Oluf Andersen, Dr. Tomas Brauner, Dr. Xuguang Huang, Professor Dr. Konstantin Klimenko, Dr. Armen Sedrakian and Professor Dr. Pengfei Zhuang for their critical reading of the manuscript and valuable suggestions. We also thank Dr. Tomas Brauner for calling our attention to erroneous expressions in Eq. (23) in the earlier version of the manuscript. The work of C. F. Mu and Y. X. Liu was supported by the National Natural Science Foundation of China under Contract Nos. 10425521 and 10935001, the Major State Basic Research Development Program under Contract Nos. G2007CB815000. C. F. Mu also acknowledges the extra financial support from China Postdoctoral Science Foundation No. 20090460168. The work of L. He was supported by the Alexander von Humboldt Foundation.

[1] R. Rapp, T. Schäfer, E. V. Shuryak, and M. Velkovsky, Phys. Rev. Lett. **81**, 53 (1998); M. Alford, K. Rajagopal, and F. Wilczek, Phys. Lett. B **422**, 247 (1998); M. Alford, K. Rajagopal, and F. Wilczek, Nucl. Phys. **B537**, 443 (1999); D. T. Son, Phys. Rev. D **59**, 094019 (1999); R. D. Pisarski and D. H. Rischke, Phys. Rev. D **61**, 074017 (2000).

[2] M. Alford, K. Rajagopal, T. Schäfer, and A. Schmitt, Rev. Mod. Phys. **80**, 1455 (2008); K. Rajagopal and F. Wilczek, arXiv:hep-ph/0011333; D. K. Hong, Acta Phys. Pol. B **32**, 1253 (2001); M. Alford, Annu. Rev. Nucl. Part. Sci. **51**, 131 (2001); T. Schäfer, arXiv:hep-ph/0304281; D. H. Rischke, Prog. Part. Nucl. Phys. **52**, 197 (2004); H.-C. Ren, arXiv:hep-ph/0404074; M. Huang, Int. J. Mod. Phys. E **14**, 675 (2005); I. A. Shovkovy, Found. Phys. **35**, 1309 (2005); Q. Wang, arXiv:0912.2485.

[3] F. Karsch, Lect. Notes Phys. **583**, 209 (2002); S. Muroya, A. Nakamura, C. Nonaka, and T. Takaishi, Prog. Theor. Phys. **110**, 615 (2003).

[4] D. T. Son and M. A. Stephanov, Phys. Rev. Lett. **86**, 592 (2001); Phys. At. Nucl. **64**, 834 (2001).

[5] J. B. Kogut, D. K. Sinclair, Phys. Rev. D **66**, 034505 (2002); **66**, 014508 (2002); **70**, 094501 (2004); P. Forcrand, M. A. Stephanov, and U. Wenger, Proc. Sci., LAT2007 (2007) 237.

[6] D. Toublan and J. B. Kogut, Phys. Lett. B **564**, 212 (2003); M. Frank, M. Buballa, and M. Oertel, Phys. Lett. B **562**, 221 (2003); M. Loewe and C. Villavicencio, Phys. Rev. D **67**, 074034 (2003); A. Barducci, R. Casalbuoni, G. Pettini, and L. Ravagli, Phys. Rev. D **69**, 096004 (2004); **71**, 016011 (2005); H. J. Warringa, D. Boer, and J. O. Andersen, Phys. Rev. D **72**, 014015 (2005); Z. Zhang and Y. X. Liu, Phys. Rev. C **75**, 064910 (2007); J. O. Andersen, Phys. Rev. D **75**, 065011 (2007); S. Shu and J. R. Li, J. Phys. G **34**, 2727 (2007); P. Kovacs and Zs. Szep, Phys. Rev. D **77**, 065016 (2008); T. Herpay and P. Kovacs, Phys. Rev. D **78**, 116008 (2008); J. Xiong, M. Jin, and J. Li, J. Phys. G **36**, 125005 (2009).

[7] L. He, M. Jin, and P. Zhuang, Phys. Rev. D **71**, 116001 (2005); L. He and P. Zhuang, Phys. Lett. B **615**, 93 (2005); L. He, M. Jin, and P. Zhuang, Mod. Phys. Lett. A **22**, 637 (2007).

[8] P. Basu, J. He, A. Mukherjee, and H.-H. Shi, J. High Energy Phys. 11 (2009) 070; J. Erdmenger, M. Kaminski, P. Kerner, and F. Rust, J. High Energy Phys. 11 (2008) 031; J. Erdmenger, M. Kaminski, and F. Rust, Phys. Rev. D **77**, 046005 (2008); K.-il Kim, Y. Kim, and S. H. Lee, arXiv:0709.1772.

[9] L. He, M. Jin, and P. Zhuang, Phys. Rev. D **74**, 036005 (2006).

[10] G. Sun, L. He, and P. Zhuang, Phys. Rev. D **75**, 096004 (2007).

[11] M. Matsuzaki, Phys. Rev. D **82**, 016005 (2010).

[12] Y. Nambu and G. Jona-Lasinio, Phys. Rev. **122**, 345 (1961); **124**, 246 (1961).

[13] D. M. Eagles, Phys. Rev. **186**, 456 (1969); A. J. Leggett, in *Modern Trends in the Theory of Condensed Matter* (Springer-Verlag, Berlin, 1980); P. Nozieres and S. Schmitt-Rink, J. Low Temp. Phys. **59**, 195 (1985); C. A. R. Sa de Melo, M. Randeria, and J. R. Engelbrecht, Phys. Rev. Lett. **71**, 3202 (1993); J. R. Engelbrecht, M. Randeria, and C. A. R. Sa de Melo, Phys. Rev. B **55**, 15153 (1997); Q. Chen, J. Stajic, S. Tan, and K. Levin, Phys. Rep. **412**, 1 (2005).

[14] M. Greiner, C. A. Regal, and D. S. Jin, Nature (London) **426**, 537 (2003); M. W. Zwierlein *et al.*, Nature (London) **435**, 1047 (2005).

[15] Y. Nishida and H. Abuki, Phys. Rev. D **72**, 096004 (2005); H. Abuki, Nucl. Phys. **A791**, 117 (2007); J. Deng, A. Schmitt, and Q. Wang, Phys. Rev. D **76**, 034013 (2007); J. Deng, J. C. Wang, and Q. Wang, Phys. Rev. D **78**, 034014 (2008); L. He and P. Zhuang, Phys. Rev. D **75**, 096003 (2007); M. Kitazawa, D. H. Rischke, and I. A. Shovkovy, Phys. Lett. B **663**, 228 (2008); H. Abuki and T. Brauner, Phys. Rev. D **78**, 125010 (2008); T. Brauner, Phys. Rev. D **77**, 096006 (2008); D. Blaschke and D. Zablocki, Phys. Part. Nucl. **39**, 1016 (2008); B. Chatterjee, H. Mishra, and A. Mishra, Phys. Rev. D **79**, 014003 (2009); H. Guo, C.-C. Chien, and Y. He, Nucl. Phys. **A823**, 83 (2009); T. Brauner, K. Fukushima, and Y. Hidaka, Phys. Rev. D **80**, 074035 (2009).

[16] M. Kitazawa, T. Koide, T. Kunihiro, and Y. Nemoto, Phys. Rev. D **65**, 091504 (2002); **70**, 056003 (2004); L. He and P. Zhuang, Phys. Rev. D **76**, 056003 (2007).

[17] B. S. Chandrasekhar, Appl. Phys. Lett. **1**, 7 (1962); A. M. Clogston, Phys. Rev. Lett. **9**, 266 (1962).

[18] P. Fulde and R. A. Ferrell, Phys. Rev. **135**, A550 (1964).

[19] A. I. Larkin and Yu. N. Ovchinnikov, Sov. Phys. JETP **20**, 762 (1965).

[20] M. Alford, J. Berges, and K. Rajagopal, Nucl. Phys. **B558**, 219 (1999); Phys. Rev. Lett. **84**, 598 (2000); M. Alford, J. A. Bowers, and K. Rajagopal, Phys. Rev. D **63**, 074016 (2001); A. K. Leibovich, K. Rajagopal, and E. Shuster, Phys. Rev. D **64**, 094005 (2001); M. Alford and K. Rajagopal, J. High Energy Phys. 06 (2002) 031.

[21] M. Huang, P. Zhuang, and W. Chao, Phys. Rev. D **67**, 065015 (2003); I. A. Shovkovy and M. Huang, Phys. Lett. B **564**, 205 (2003); M. Huang and I. A. Shovkovy, Nucl. Phys. **A729**, 835 (2003); S. B. Ruester, I. A. Shovkovy, and D. H. Rischke, Nucl. Phys. **A743**, 127 (2004); M. Alford, C. Kouvaris, and K. Rajagopal, Phys. Rev. Lett. **92**, 222001 (2004); Phys. Rev. D **71**, 054009 (2005); S. B. Ruster, V. Werth, M. Buballa, I. A. Shovkovy, and D. H. Rischke, Phys. Rev. D **72**, 034004 (2005); D. Blaschke, S. Fredriksson, H. Grigorian, A. M. Oztas, and F. Sandin, Phys. Rev. D **72**, 065020 (2005); H. Abuki and T. Kunihiro, Nucl. Phys. **A768**, 118 (2006).

[22] M. Huang and I. A. Shovkovy, Phys. Rev. D **70**, 051501 (2004); **70**, 094030 (2004); R. Casalbuoni, R. Gatto, M. Mannarelli, G. Nardulli, and M. Ruggieri, Phys. Lett. B **605**, 362 (2005); M. Alford and Q. Wang, J. Phys. G **31**, 719 (2005); **32**, 63 (2006); K. Fukushima, Phys. Rev. D **72**, 074002 (2005); **73**, 094016 (2006); K. Iida and K. Fukushima, Phys. Rev. D **74**, 074020 (2006); I. Giannakis and H. Ren, Phys. Lett. B **611**, 137 (2005); Nucl. Phys. **B723**, 255 (2005); I. Giannakis, D. Hou, and H. C. Ren, Phys. Lett. B **631**, 16 (2005); M. Huang, Phys. Rev. D **73**, 045007 (2006); E. V. Gorbar, M. Hashimoto, and V. A. Miransky, Phys. Lett. B **632**, 305 (2006); Phys. Rev. Lett. **96**, 022005 (2006); I. Giannakis, D. Hou, M. Huang, and H. C. Ren, Phys. Rev. D **75**, 011501 (2007); **75**, 014015

(2007); O. Kiriyama, D. H. Rischke, and I. A. Shovkovy, Phys. Lett. B **643**, 331 (2006); O. Kiriyama, Phys. Rev. D **74**, 074019 (2006); **74**, 114011 (2006); L. He, M. Jin, and P. Zhuang, Phys. Rev. D **75**, 036003 (2007); A. Sedrakian and D. H. Rischke, Phys. Rev. D **80**, 074022 (2009).

[23] D. Ebert and K. G. Klimenko, J. Phys. G **32**, 599 (2006); Eur. Phys. J. C **46**, 771 (2006); H. Abuki, R. Anglani, R. Gatto, M. Pellicoro, and M. Ruggieri, Phys. Rev. D **79**, 034032 (2009); H. Abuki, T. Brauner, and H. J. Warringa, Eur. Phys. J. C **64**, 123 (2009); D. Ebert and K. G. Klimenko, Phys. Rev. D **80**, 125013 (2009); J. O. Andersen and L. Kyllingstad, J. Phys. G **37**, 015003 (2010).

[24] M. W. Zwierlein *et al.*, Science **311**, 492 (2006); G. B. Partridge *et al.*, Science **311**, 503 (2006); M. W. Zwierlein *et al.*, Nature (London) **442**, 54 (2006); Y. Shin, M. W. Zwierlein, C. H. Schunck, A. Schirotzek, and W. Ketterle, Phys. Rev. Lett. **97**, 030401 (2006).

[25] D. T. Son and M. A. Stephanov, Phys. Rev. A **74**, 013614 (2006).

[26] D. E. Sheehy and L. Radzihovsky, Phys. Rev. Lett. **96**, 060401 (2006); Ann. Phys. (N.Y.) **322**, 1790 (2007).

[27] H. Hu and X. J. Liu, Phys. Rev. A **73**, 051603 (2006).

[28] M. Mannarelli, G. Nardulli, and M. Ruggieri, Phys. Rev. A **74**, 033606 (2006).

[29] P. F. Bedaque, H. Caldas, and G. Rupak, Phys. Rev. Lett. **91**, 247002 (2003); T. D. Cohen, Phys. Rev. Lett. **95**, 120403 (2005); J. Carlson and S. Reddy, Phys. Rev. Lett. **95**, 060401 (2005); A. Sedrakian, J. Mur-Petit, A. Polls, and H. Muether, Phys. Rev. A **72**, 013613 (2005); M. Iskin and C. A. R. Sa de Melo, Phys. Rev. Lett. **97**, 100404 (2006); L. He, M. Jin, and P. Zhuang, Phys. Rev. B **73**, 214527 (2006); **74**, 214516 (2006); C. Lobo, A. Recati, S. Giorgini, and S. Stringari, Phys. Rev. Lett. **97**, 200403 (2006); J. Kinnunen, L. M. Jensen, and P. Torma, Phys. Rev. Lett. **96**, 110403 (2006); K. Machida, T. Mizushima, M. Ichioka, Phys. Rev. Lett. **97**, 120407 (2006); T. N. De Silva and E. J. Mueller, Phys. Rev. A **73**, 051602 (2006); Phys. Rev. Lett. **97**, 070402 (2006); Hui Hu, X. J. Liu, P. D. Drummond, Phys. Rev. Lett. **98**, 070403 (2007); G. Orso, Phys. Rev. Lett. **98**, 070402 (2007).

[30] G. Sarma, J. Phys. Chem. Solids **24**, 1029 (1963).

[31] W. V. Liu and F. Wilczek, Phys. Rev. Lett. **90**, 047002 (2003).

[32] M. M. Forbes, E. Gubankova, W. V. Liu, and F. Wilczek, Phys. Rev. Lett. **94**, 017001 (2005).

[33] S. T. Wu and S. Yip, Phys. Rev. A **67**, 053603 (2003).

[34] D. E. Sheehy and L. Radzihovsky, Phys. Rev. B **75**, 136501 (2007).

[35] U. Vogl and W. Weise, Prog. Part. Nucl. Phys. **27**, 195 (1991); S. P. Klevansky, Rev. Mod. Phys. **64**, 649 (1992); T. Hatsuda and T. Kunihiro, Phys. Rep. **247**, 221 (1994).

[36] M. Buballa, Phys. Rep. **407**, 205 (2005).

[37] M. Asakawa and K. Yaza, Nucl. Phys. **A504**, 668 (1989); A. Barducci, R. Casalbuoni, S. De Curtis, R. Gatto, and G. Pettini, Phys. Rev. D **41**, 1610 (1990); P. Zhuang, J. Hufner, and S. P. Klevansky, Nucl. Phys. **A576**, 525 (1994).

[38] U. Lombardo, P. Nozieres, P. Schuck, H.-J. Schulze, and A. Sedrakian, Phys. Rev. C **64**, 064314 (2001); E. Gubankova, A. Schmitt, and F. Wilczek, Phys. Rev. B **74**, 064505 (2006); M. Kitazawa, D. Rischke, and A. Shovkovy, Phys. Lett. B **637**, 367 (2006).

[39] L. He, Y. Jiang, and P. Zhuang, Phys. Rev. C **79**, 045205 (2009).

[40] R. F. Sawyer, Phys. Rev. Lett. **29**, 382 (1972); D. J. Scalapino, Phys. Rev. Lett. **29**, 386 (1972); G. Baym, Phys. Rev. Lett. **30**, 1340 (1973); D. K. Campbell, R. F. Dashen, and J. T. Manassah, Phys. Rev. D **12**, 979 (1975); **12**, 1010 (1975).

[41] A. A. Abrikosov, *Fundamental Theory of Metals* (North-Holland, Amsterdam, 1988), pp 111–114G. E. Volovik, *Exotic Properties of Superfluid* ^{3}He (World Scientific, Singapore, 1992); G. E. Volovik, arXiv:cond-mat/0601372.

[42] R. D. Duncan and C. A. R. Sa de Melo, Phys. Rev. B **62**, 9675 (2000); S. S. Botelho and C. A. R. Sa de Melo, J. Low Temp. Phys. **140**, 409 (2005); M. Iskin and C. A. R. Sa de Melo, Phys. Rev. A **74**, 013608 (2006).

[43] L. Chang, Y. X. Liu, M. S. Bhagwat, C. D. Roberts, and S. V. Wright, Phys. Rev. C **75**, 015201 (2007).

[44] H. Chen, W. Yuan, L. Chang, Y. X. Liu, T. Klaehn, and C. D. Roberts, Phys. Rev. D **78**, 116015 (2008); H. Chen, W. Yuan, and Y. X. Liu, J. Phys. G **36**, 064073 (2009).

[45] R. Casalbuoni and G. Nardulli, Rev. Mod. Phys. **76**, 263 (2004).

[46] J. O. Andersen and T. Brauner, Phys. Rev. D **81**, 096004 (2010).

[47] D. Nickel and M. Buballa, Phys. Rev. D **79**, 054009 (2009); M. Buballa and D. Nickel, arXiv:0911.2333.

[48] T. Fujihara, D. Kimura, T. Inagaki, and A. Kvinikhidze, Phys. Rev. D **79**, 096008 (2009).

[49] K. Fukushima and K. Iida, Phys. Rev. D **76**, 054004 (2007).

[50] F. Fumarola, I. L. Aleiner, and B. L. Altshuler, arXiv:cond-mat/0703003; L. He and P. Zhuang, Phys. Rev. A **78**, 033613 (2008).